INVESTIGATION OF ELECTRON IMPACT PROCESSES RELEVANT TO VISIBLE LASERS

12
B.S.

M. John W. Boness and H. A. Hyman
Avco Everett Research Laboratory, Inc.
2385 Revere Beach Parkway
Everett, MA 02149

Final Technical Report for Period 15 August 1974 to 14 November 1977

APPROVED FOR PUBLIC RELEASE; DISTRIBUTION UNLIMITED.

Sponsored by
DEFENSE ADVANCED RESEARCH PROJECTS AGENCY
DARPA Order No. 1806

Monitored by
OFFICE OF NAVAL RESEARCH
DEPARTMENT OF THE NAVY
Arlington, VA 22217

FOREWORD

Contract No. : N00014-75-C-0064

DARPA Order No. : 1806

Program Code No. : 5E20

Short Title of Work: Investigation of Electron Impact Processes
Relevant to Visible Lasers

Contractor: Avco Everett Research Laboratory, Inc.
2385 Revere Beach Parkway
Everett, MA 02149

Principal Investigator: Mr. John W. Boness
(617) 389-3000, Ext. 451

Scientific Officer: Director, Physics Program, Physical Sciences Division
Office of Naval Research
800 North Quincy Street
Arlington, VA 22217

Effective Date of Contract: 15 August 1974

Contract Expiration Date: 14 November 1977

Amount of Contract: $605, 222

UNCLASSIFIED

SECURITY CLASSIFICATION OF THIS PAGE (When Data Entered)

REPORT DOCUMENTATION PAGE

READ INSTRUCTIONS BEFORE COMPLETING FORM

1. REPORT NUMBER

2. GOVT ACCESSION NO.

3. RECIPIENT'S CATALOG NUMBER

9

4. TITLE (and Subtitle)

6 Investigation of Electron Impact Processes Relevant to Visible Lasers

5. TYPE OF REPORT & PERIOD COVERED

Final Technical Report
15 Aug [redacted]74 – 14 Nov [redacted]77

6. PERFORMING ORG. REPORT NUMBER

7. AUTHOR(s)

14 M. John W. Boness [redacted] H. A. Hyman

8. CONTRACT OR GRANT NUMBER(s)

15 N00014-75-C-0064, DARPA Order-1806

9. PERFORMING ORGANIZATION NAME AND ADDRESS

Avco Everett Research Laboratory, Inc.
2385 Revere Beach Parkway
Everett, Ma 02149

10. PROGRAM ELEMENT, PROJECT, TASK AREA & WORK UNIT NUMBERS

11. CONTROLLING OFFICE NAME AND ADDRESS

Defense Advanced Research Projects Agency
DARPA Order No. 1806

12. REPORT DATE

11 24 Nov 77

13. NUMBER OF PAGES

74

12 78 p.

14. MONITORING AGENCY NAME & ADDRESS (if different from Controlling Office)

Office of Naval Research
Department of the Navy
Arlington, VA 22217

15. SECURITY CLASS. (of this report)

Unclassified

15a. DECLASSIFICATION/DOWNGRADING SCHEDULE

16. DISTRIBUTION STATEMENT (of this Report)

Approved for Public Release; Distribution Unlimited.

17. DISTRIBUTION STATEMENT (of the abstract entered in Block 20, if different from Report)

18. SUPPLEMENTARY NOTES

19. KEY WORDS (Continue on reverse side if necessary and identify by block number)

Visible Laser
Metastable Atom, Cross Section, Electron
Argon
Krypton
Electron Spectroscopy
Born Calculations
Intermediate Coupling
Strong Coupling

20. ABSTRACT (Continue on reverse side if necessary and identify by block number)

This report describes the results of a combined experimental and theoretical program to determine the electron impact excitation cross sections of metastable argon and krypton atoms to higher lying states. This research has particular significance with regard to rare gas excimer laser research.

During the course of the experimental program a crossed beams apparatus was constructed which employed a glow discharge source of metastable

Φ48 45Φ

yields

(20)

rare gas atoms. Initially the technique of electron spectroscopy was employed as the diagnostic, however, this was later replaced by fluorescence spectroscopy. Signal-to-noise problems restricted the scope of the measurements, however measurements were made for certain transitions of the type e + Kr 5 sj $\rightarrow$ e + Kr 5 pj' and e + Ar 4sj $\rightarrow$ e + Ar 4 pj'. Measurements were also made for ground state excitation cross sections corresponding to line excitation of Kr 5p $\rightarrow$ 5s and Ar 4p $\rightarrow$ 4s transitions. In the case of krypton only one other set of published cross section data for these transitions exists in the literature.

yields

The accuracy of the metastable excitation measurements was limited by signal-to-noise considerations and by uncertainties in the determination of the metastable density in the atomic beam. For krypton the results indicate that the cross section for all transitions contained within the 5s $\rightarrow$ 5p manifold is greater than 5×10^{-15} cm^2.

The theoretical program involved calculations of Born cross section for electron impact excitation of metastable levels of argon and krypton to higher-lying states. The results showed that the intermediate coupling representation must be used to obtain reliable results. An approximate treatment of strong coupling effects was included for the dominant ns - np transitions, and the applicable range and validity of the Born calculation was considered. The results show that the excitation cross sections from the metastable levels to the next excited state Ar 4s $\rightarrow$ 4p and Kr 5s $\rightarrow$ 5p are extremely large, of the order 10^{-14} cm^2.

TABLE OF CONTENTS

LIST OF ILLUSTRATIONS

I. INTRODUCTION

The role of the Avco Everett Research Laboratory, Inc. (AERL) Electron Kinetics program in the DARPA/ONR sponsored AERL visible laser program is to supply relevant electron kinetics data necessary for modeling and optimizing laser performance specifically in the important areas of the KrF scaleup, the excimer laser research program and the area of small-scale discharge studies.

The advent of techniques developed at AERL for scaling electric gas discharges to large volumes and to high volumetric pumping rates revealed a considerable lack of electron scattering cross section data required to model and, hence, understand these discharges. In particular, since these discharges are often characterized by very high electron pumping rates in order to achieve laser systems capable of being scaled to high-average power, then the fraction of excited species is large and electron collisions with such species is known to play a major role in affecting the overall electron kinetics of the discharge. [1]

Due to the problems associated with the preparation and manipulation of excited atomic and molecular species for the purposes of performing electron collision experiments and also due to the previous lack of any important practical application of the data, the total data available

(1) "KrF Laser Research," AERL 804, April 1976.

describing such collisions is rather meager. The situation has improved somewhat recently as a growing recognition of the practical importance of these processes develops.[(2-6)]

The AERL Electron Kinetics program was proposed in order to provide absolute cross section data, particularly, with regard to collision processes between electrons and excited atomic and molecular species. The program consists of parallel and complementary experimental and theoretical efforts.

The goal of these combined program efforts is to provide reliable absolute cross section data covering range of electron energies encountered in the electric discharges of interest.

In addition to the complementary benefits offered by the experimental and theoretical efforts, each has certain capabilities not shared by the other. For instance, the theoretical effort is not restricted to metastable excited species as is the experimental technique. It can also be applied to allowed transitions from excited species, which can also reach high densities in the discharge due to radiative trapping and hence effectively exhibit metastable properties. The experimental program on the other hand can handle processes in ground state or metastable molecular species for which accurate wavefunctions are not available and are therefore not amenable to the theory.

---

(2) Long, D. R. and Geballe, R., Phys. Rev. 1, 260 (1970).

(3) Lake, M. L. and Garscadden, A., 28th Gaseous Electronics Conference, Rolla, Mo. (1975), Paper C-5.

(4) Mityurwa, A. A. and Penkin, N. P., Opt. Spectrosc. 38, 229 (1975).

(5) Wilson, W. G. and Williams, W. L., J. Phys. B9, 423 (1976).

(6) Tanne, P. D., "Cumulative Ionization and Excitation of Molecular Nitrogen Metastables by Electron Impact," Dissertation (1973), School of Engineering, Air Force Institute of Technology.

The rare gas monohalide laser systems which have been the subject of extensive experimental and theoretical investigations at AERL[7,8,9] have emerged as extremely promising candidates for satisfying certain goals of the DARPA visible laser program. These studies have identified electron collision processes with metastable states of the rare gas atom constituents as playing a major role in both discharge stability and in determining the equilibrium metastable concentration, which through reaction with the halogen molecule leads to excimer formation.

Therefore, the specific goal of the AERL electron kinetics program is to provide absolute cross sections for electron collisions with the first excited states of the rare gases argon and krypton, both for the metastable substates and for the substates which are optically connected to the ground state.

Examples of the transitions of interest are indicated in the partial energy level diagram of krypton shown in Figure 1 and for argon shown in Figure 2. The only theoretical calculations available for transitions of the type shown in Figures 1 and 2 which cover the energy range of interest for laser modeling are those of Burke et al.[10] for the He atom. The transitions corresponding to those shown in Figures 1 and 2 are shown in Figure 3 they are $2'S \rightarrow 2'P$ and $2^3S \rightarrow 2^3P$ transitions. The important feature of these

(7) Ewing, J. J. and Brau, C. A., Appl. Phys. Lett. 27, 350 (1975).

(8) Ewing, J. J. and Brau, C. A., Phys. Rev. A12, 129 (1975).

(9) Mangano, J.A. and Jacob, J. H., Appl. Phys. Lett. 27, 495 (1975).

(10) Burke, P.G., Cooper, J.W., Ormande, S. and Taylor, A.J., Abstract V ICPEAC, Liningrad, (1967).

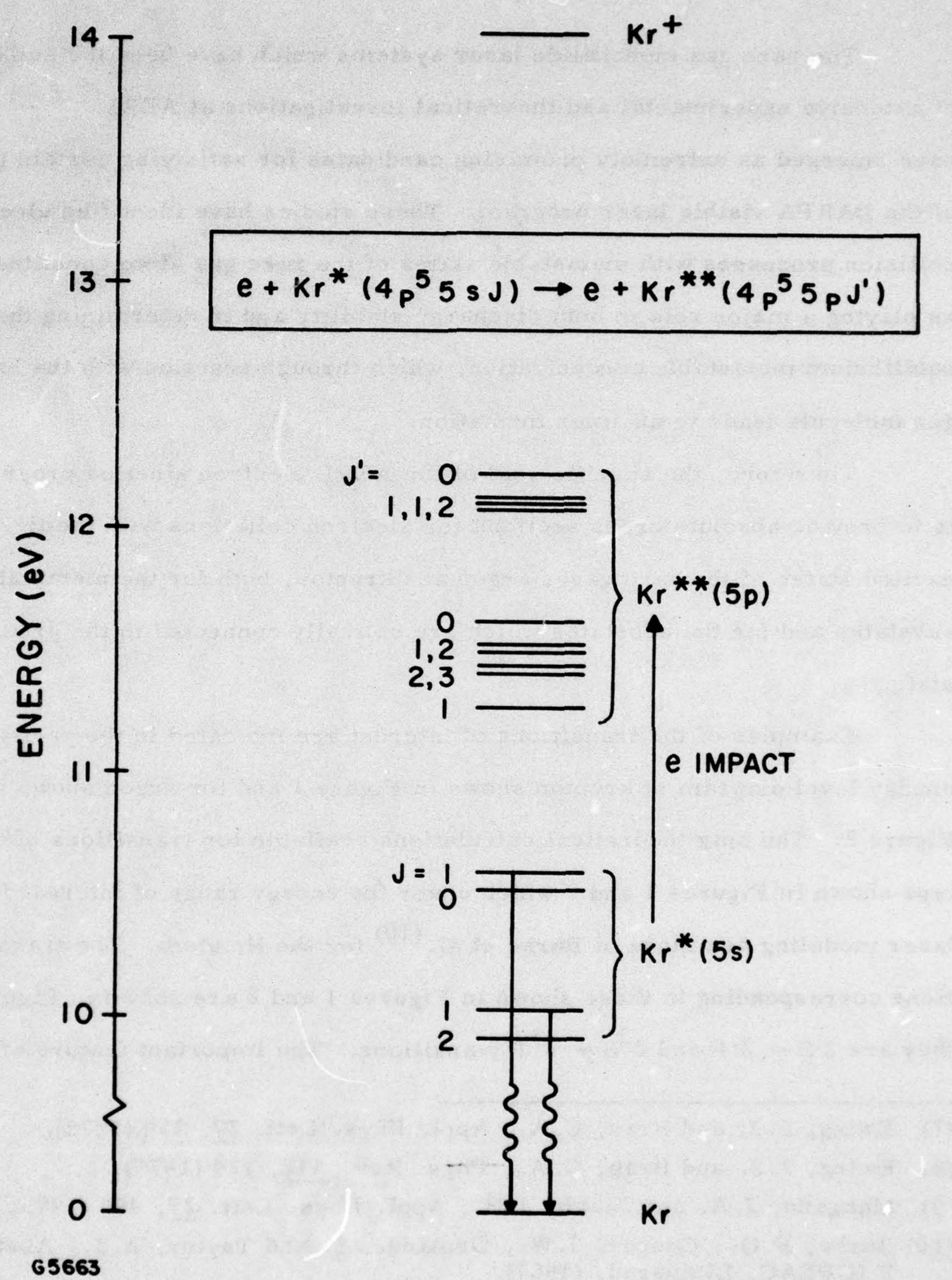

Figure 1 **Partial Energy Level Diagram of the Krypton Atom Indicating Transactions Between the First Two Excited State Manifolds**

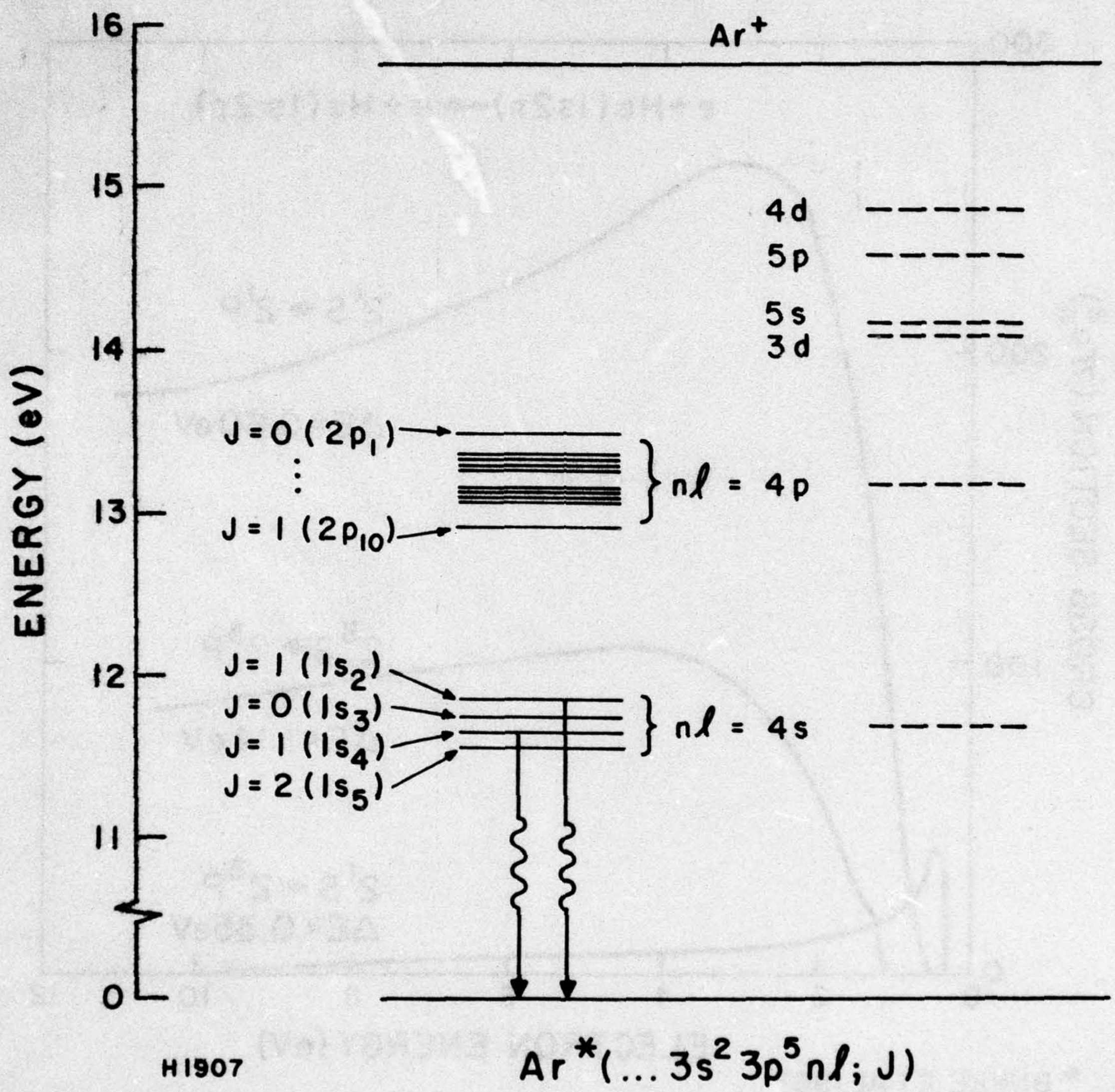

Figure 2 Partial Energy Level Diagram of the Argon Atom Indicating Transitions Between the First Two Excited State Manifolds

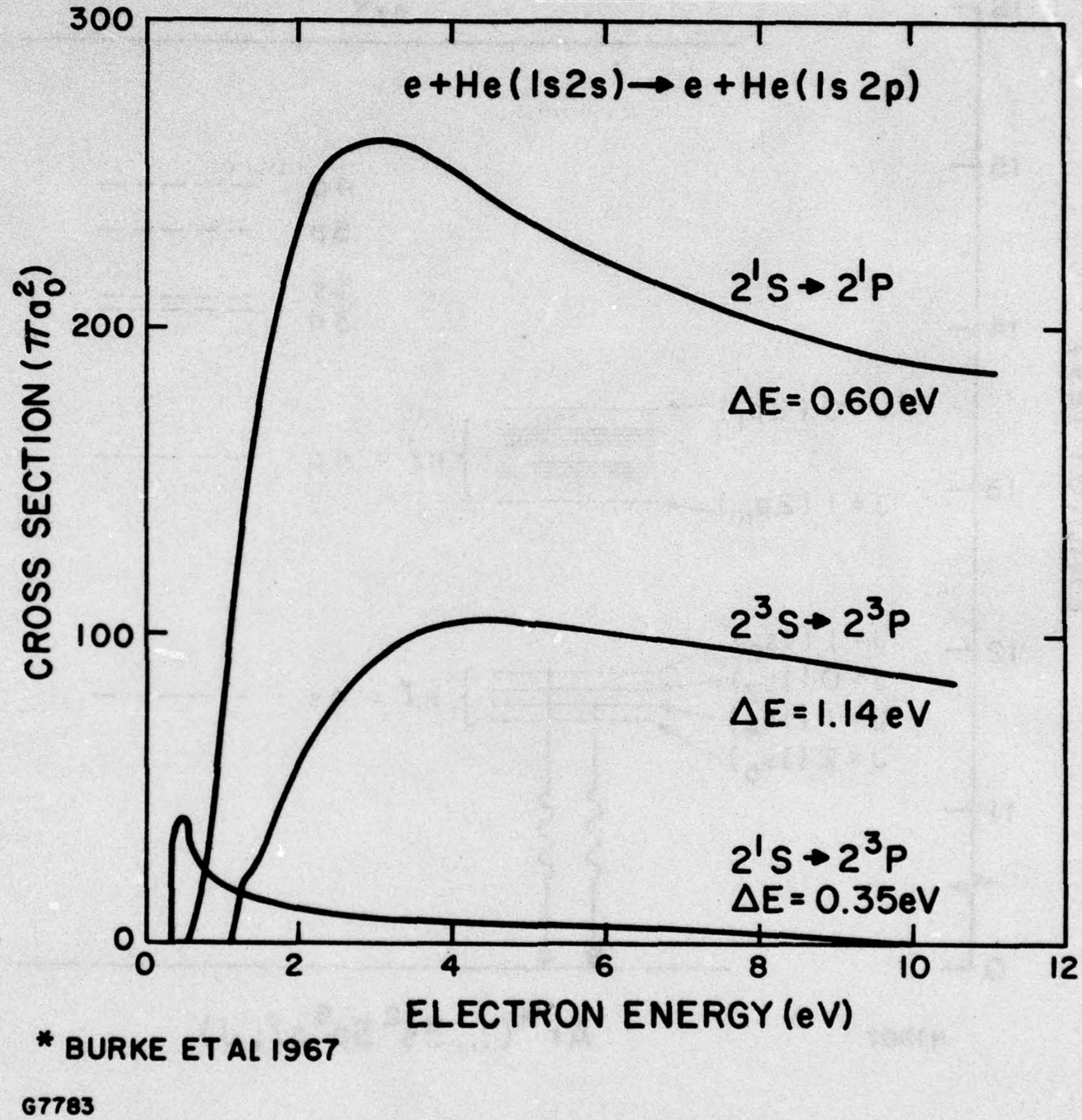

Figure 3 Close Coupling Calculations for Excitation Between the n = 2 States of Helium(10)

cross sections is the extremely large magnitude, $\sim 10^{-14}$ cm^2 which supports our contention that the corresponding transitions between the first two excited states of the other rare gases should be extremely large.

Furthermore, in terms of electronic structure, the first excited state of krypton resembles the ground state of rubidium. Thus, the electron impact excitation cross section for transitions between the first two excited states, $5s \rightarrow 5p$, in krypton should be analogous to the alkali atom resonance transition which is known to be extremely large, of the order 10^{-14} cm^2.

This value is much larger than the various cross sections involving ground state excitation processes. Consequently, once significant fractional populations of the 5s excited state are generated in the discharge then the $5s \rightarrow 5p$ excitation process will become the dominant energy loss process for the electrons and attempts to generate higher densities of the 5s state will lead to less efficient operation of the laser, and due to the close proximity of this state to the ionization limit will eventually lead to rapid stepwise ionization and consequent discharge instability.

The experimental apparatus which is described in Section II employs the crossed beams technique and was originally combined with an electron spectrometer to perform electron energy loss analysis and hence provide the required relative excitation cross sections. For reasons which have been fully discussed in a previous semi-annual report,(11) a fluorescence technique was substituded for the method of electron energy loss spectroscopy in order to identify and measure the relative excitation functions for the transitions of interest.

---

(11) "Investigation of Electron Impact Processes Relevant to Visible Lasers." Boness, M.J., and Hyman, H.A., AERL Semi-Annual Report, March 1977 - Aug. 1977.

The source of metastable atoms employed is a low pressure dc discharge tube. The source has been fully characterized and the design and operation optimized for the production of metastable gas atoms. Using an Auger metastable atom detector absolute metastable krypton densities in the region of the crossed electron and atomic beams have been estimated to be $\sim 10^7$ cm^{-3}.

Experiments are reported using the fluorescence technique to provide absolute cross sections for excitation from the metastable states for krypton.

The principal results of the theoretical calculations are: (1) the electron impact excitation of metastable argon and krypton is dominated by a single transition (4s → 4p for Ar and 5s → 5p) with a large cross section $\sim 100\ \pi a_o^2$ at the peak) and (2) strong coupling effects are dominant at low energies for the ns → np transition. In addition, it has been shown that the use of the intermediate coupling representation is required to obtain meaningful results for cross sections between the various substates.

II. EXPERIMENT

A. TECHNIQUE

The experiment employs the crossed-beams technique, the concept of which is outlined in Figure 4. A low density collimated beam of the atomic or molecular species of interest is collided at right angles with an e-beam of the appropriate energy whose energy spread is small compared with the mean energy. In general, a wide variety of diagnostic techniques can be employed to measure the electron scattering cross sections. The merits of the various methods were discussed at length in the original AERL Electron Kinetics Program Proposal, which concluded that the electron spectroscopy of the inelastically scattered electrons offered the broadest application compared to any other single technique. However, recognizing that on occasion other diagnostics might be preferred or required for certain processes, the apparatus was constructed in such a way as to permit the addition of these refinements without major modification to the system.

The experiment was enclosed within a double, differentially pumped, stainless steel vacuum chamber, bakeable to $200^{o}C$ and capable of producing an ultimate vacuum in the 10^{-8} - Torr range. A schematic of the vacuum system is shown in Figure 5. The two halves of the vacuum chamber communicate via a small orifice through which the atomic beam passes. Thus the atomic beam source and metastable excitation system are separated from the electron impact, crossed-beams region and from the electron spectrometer. Each chamber is provided with an automatic gate valve for

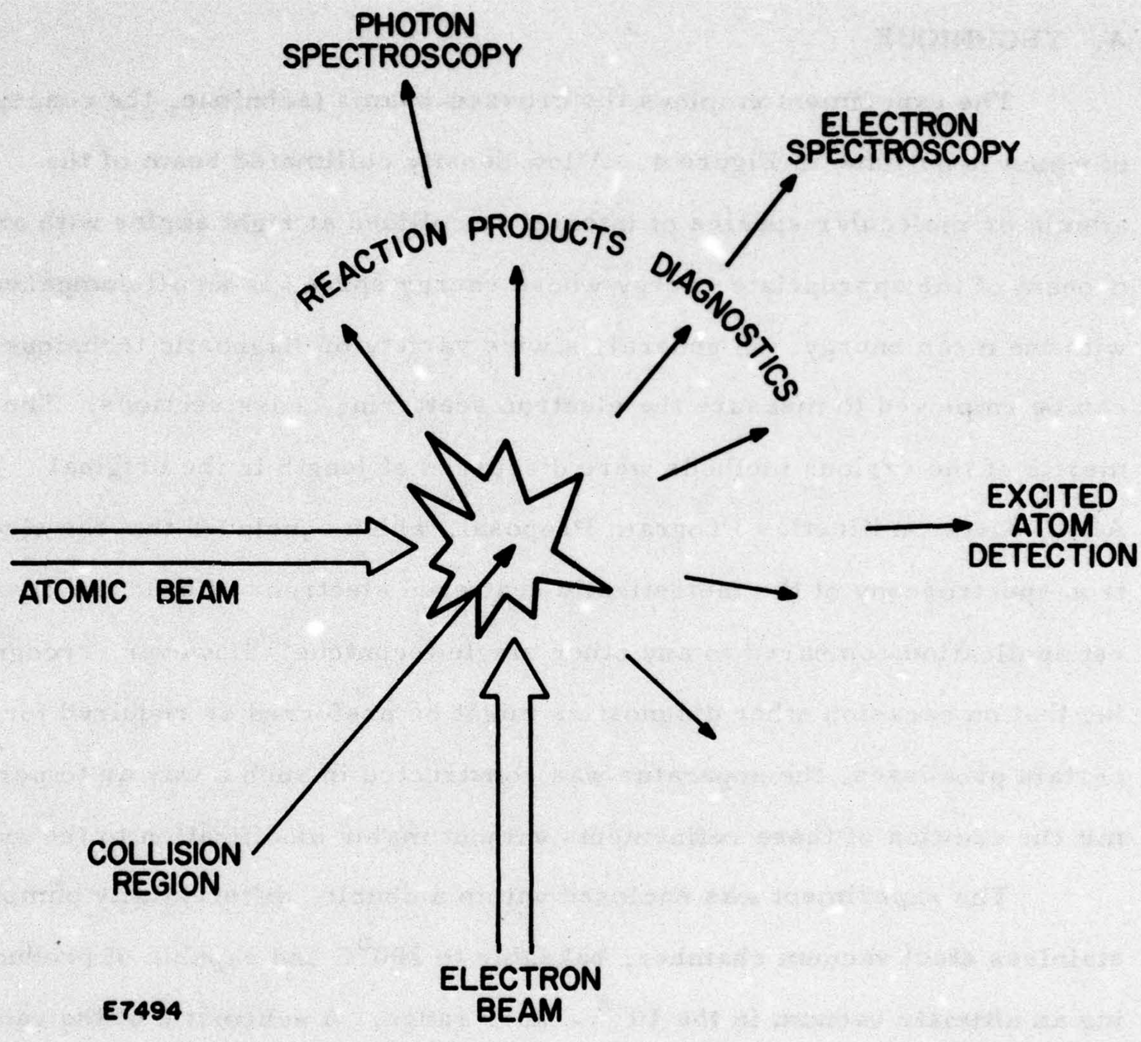

Figure 4 Concept of the Crossed Beams Technique

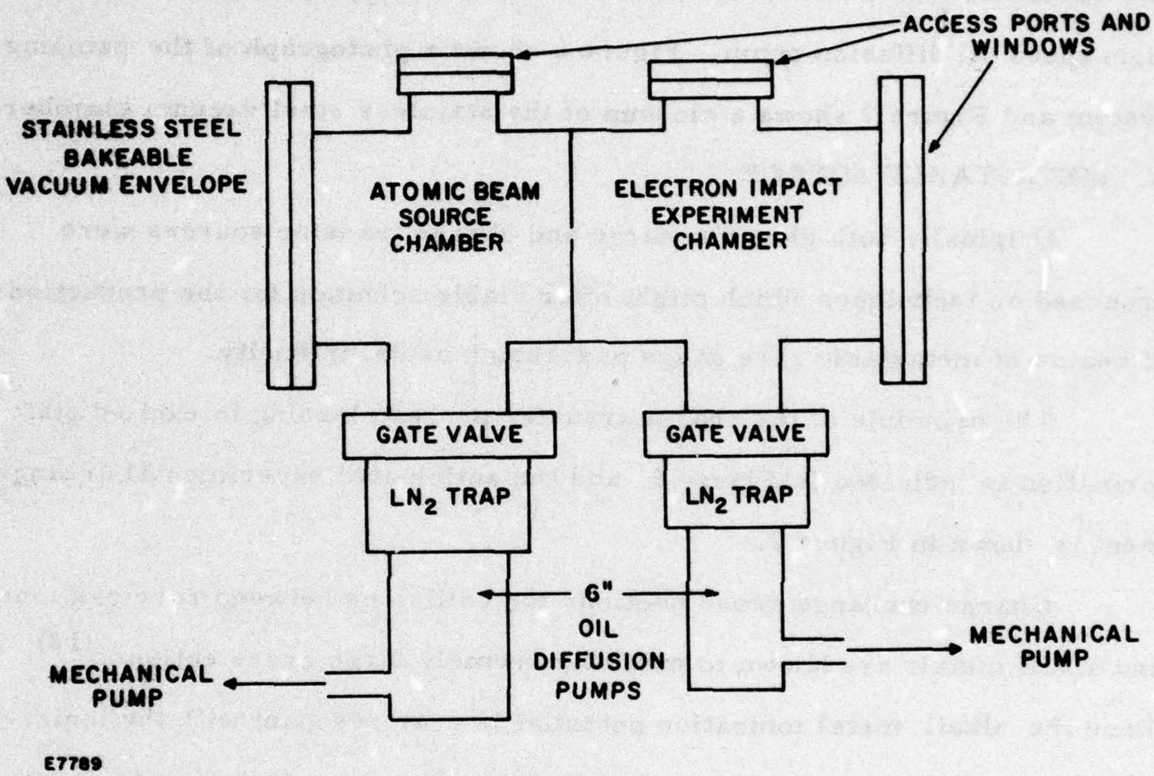

Figure 5 **Schematic of Pumping System and Vacuum Chamber**

emergency isolation in the event of power failure and also to provide rapid recycling of the system. Liquid nitrogen traps isolate the oil diffusion pumps to prevent oil backstreaming from the pumps and contaminating sensitive surfaces. Each half of the vacuum chamber is pumped by a 6-inch, high-speed oil diffusion pump. Figure 6 shows a photograph of the pumping system and Figure 7 shows a closeup of the stainless steel vacuum chamber.

B. METASTABLE SOURCE

Originally both glow discharge and charge transfer sources were proposed as techniques which might offer viable schemes for the production of beams of metastable rare gases possessing useful intensity.

The principle of the charge transfer process leading to excited state formation is indicated in Figure 8, and the anticipated experimental arrangement is shown in Figure 9.

Charge exchange cross sections for collisions between rare gas ions and alkali metals are known to exhibit extremely large cross ections.[12] Since the alkali metal ionization potential is near resonant with the ionization potential of the corresponding metastable rare gas, then it is to be expected and has, in fact, been confirmed[13] that these charge-exchange collisions are likely to produce copious amounts of metastable states of the rare gas.

Both the charge transfer and glow discharge techniques were pursued initially, however, the relative technical simplicity of the glow discharge technique has led to faster development of this source to the extent

(12) Peterson, J.R. and Lorentz, D.C., Phys. Rev. 182, 152 (1969).

(13) Neynaber, R.H. and Magnuson, G.D., J. Chem. Phys. 65, 5239 (1976).

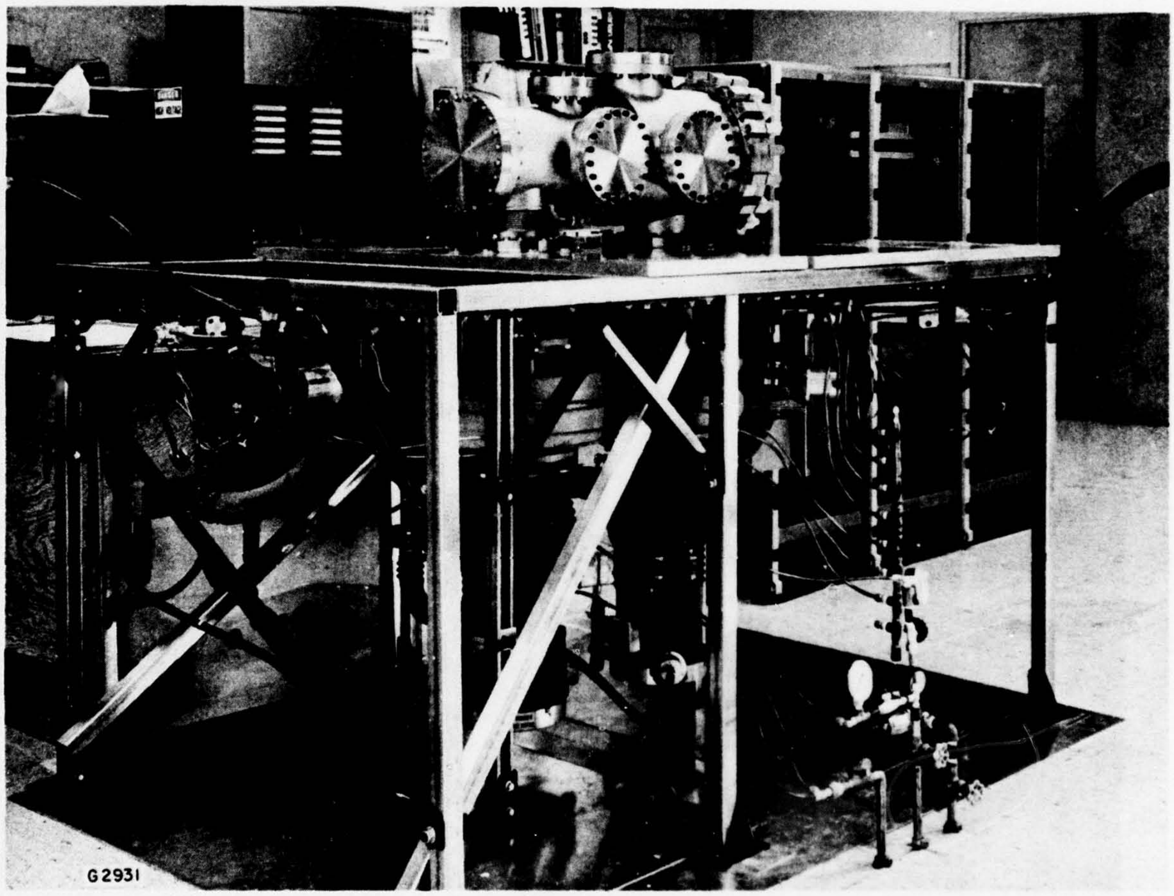

Figure 6 Photograph of Pumping System and Vacuum Chamber

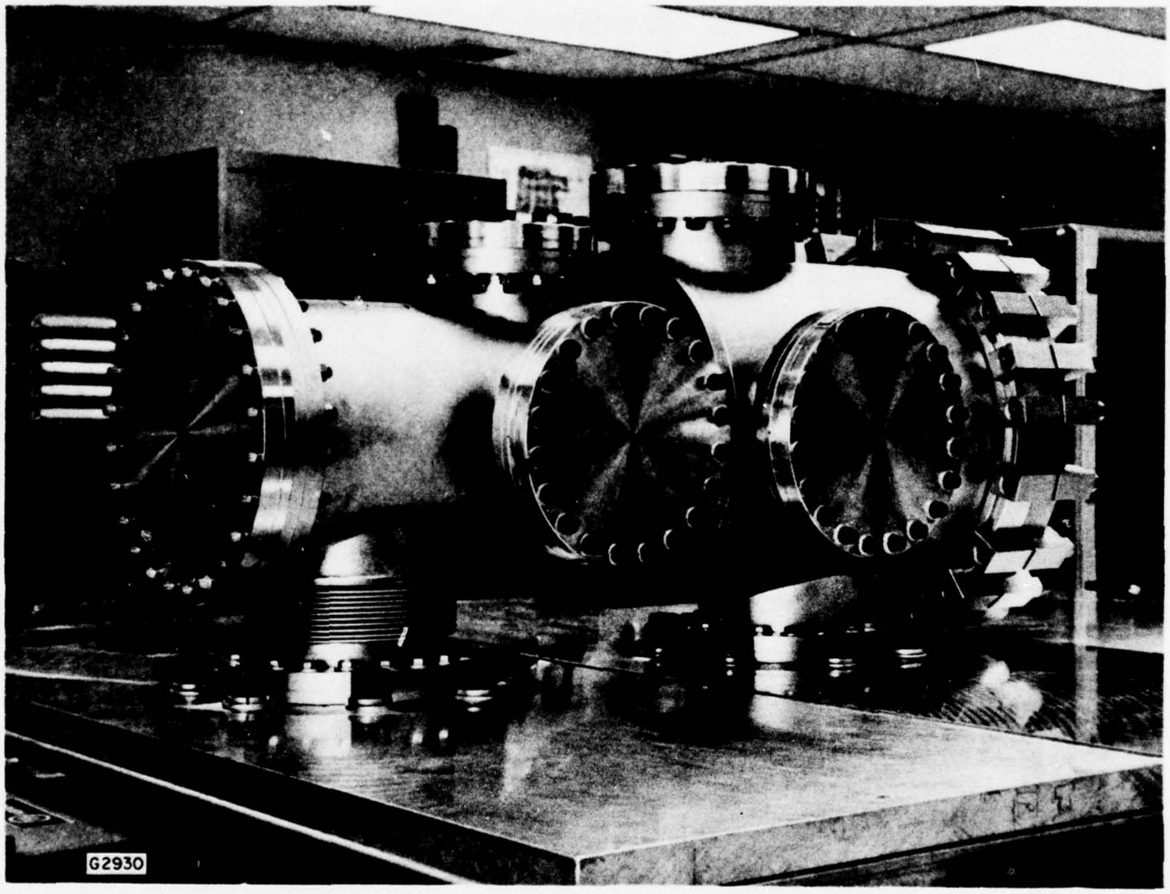

Figure 7 Photograph of Stainless Steel Vacuum Chamber Showing Side Access Ports to Metastable Source and Election Spectrometer Chamber

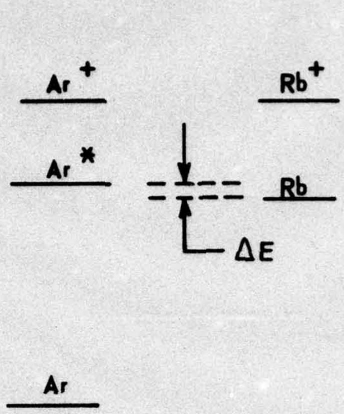

$$Ar^+ + Rb \longrightarrow Rb^+ + \begin{cases} Ar^* \\ Ar \end{cases}$$

$$\sigma \sim 1.5 \times 10^{-14}\ \mathrm{cm}^2$$

(J.R. PETERSON & D.C. LORENTS, PHYS REV, 182, 152, (1969))

BRANCHING RATIOS, γ

RARE GAS X	ALKALI	$\gamma = \dfrac{X^*}{X + X^*}$
He	Cs	0.85
Ne	Na	0.5
Ar	Rb	0.4

(R.H. NEYNABER & G.D. MAGNUSON, J. CHEM. PHYS. 65, 5239, (1976))

G7785

Figure 8 Charge Exchange Leading to Excited State Formation

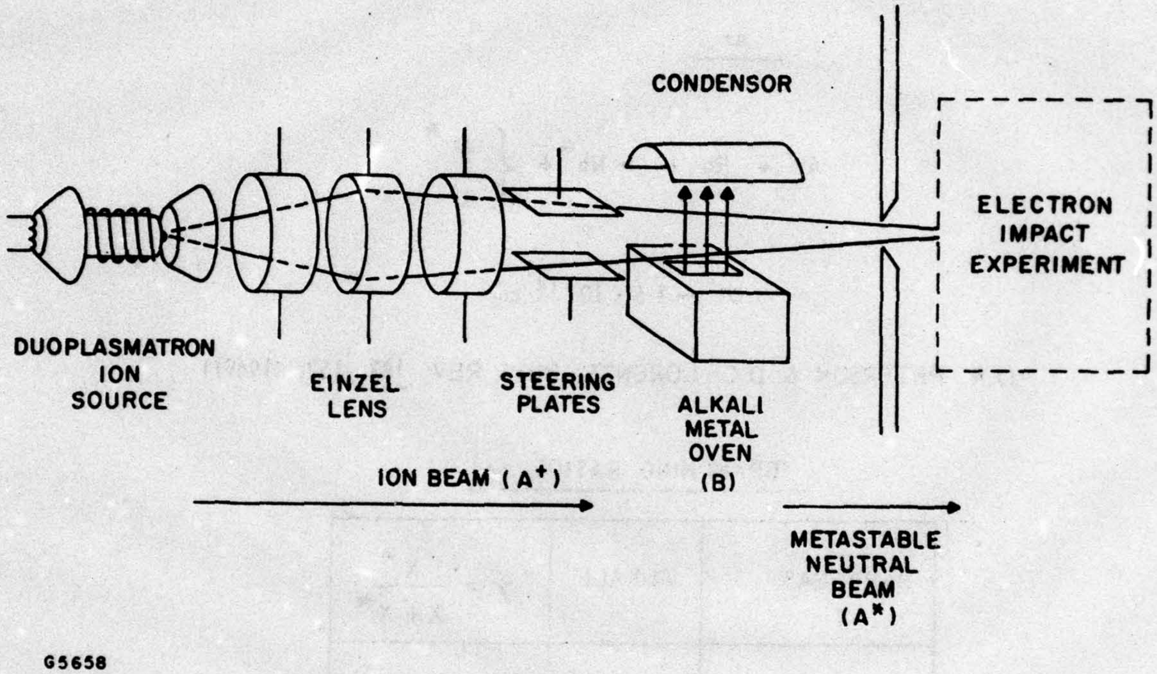

Figure 9 Schematic of the Charge Exchange Apparatus for Metastable Rare Gas Production

that an optimized design was installed in the system in order to perform the electron scattering experiments.

1. Glow Discharge Source

The principle of the glow discharge source is to simply create a low pressure stable D.C. discharge and to allow the discharge products to effuse from a small aperture located at the end of the discharge tube. The discharge tube is located in a separately pumped chamber having a pumping speed of approximately 550 ℓ/sec. This chamber communicates with the spectrometer chamber via a 0.050 inch diameter orifice. Various apertures can be placed between the discharge tube orifice and the 0.050 inch hole separating the two chambers. Bias potentials can be applied to these apertures in order to reject charged particles and to quench high lying, long lived Rydberg states in the beam. Thus, in principle, it is possible to extract a quasi - atomic beam through the 0.050 inch aperture which contains only ground state atoms and the required metastable atoms.

The developmental work leading to an optimized design of glow discharge source has been completely described in a previous semi-annual report.[11]

A variety of discharge sources were investigated and the f nal design adopted is shown in Figure 10. The source consists of a short discharge tube approximately two inches long which is closed at one end by a glass plate carrying a 0.020 inch diameter hole. The discharge anode was placed beyond the end of the 0.020 inch aperture so that the discharge was constricted by the 0.020 inch operature prior to reaching the anode. This constriction was found to be the key feature for optimizing metastable production. Maintaining a short discharge length was found to reduce the photon component.

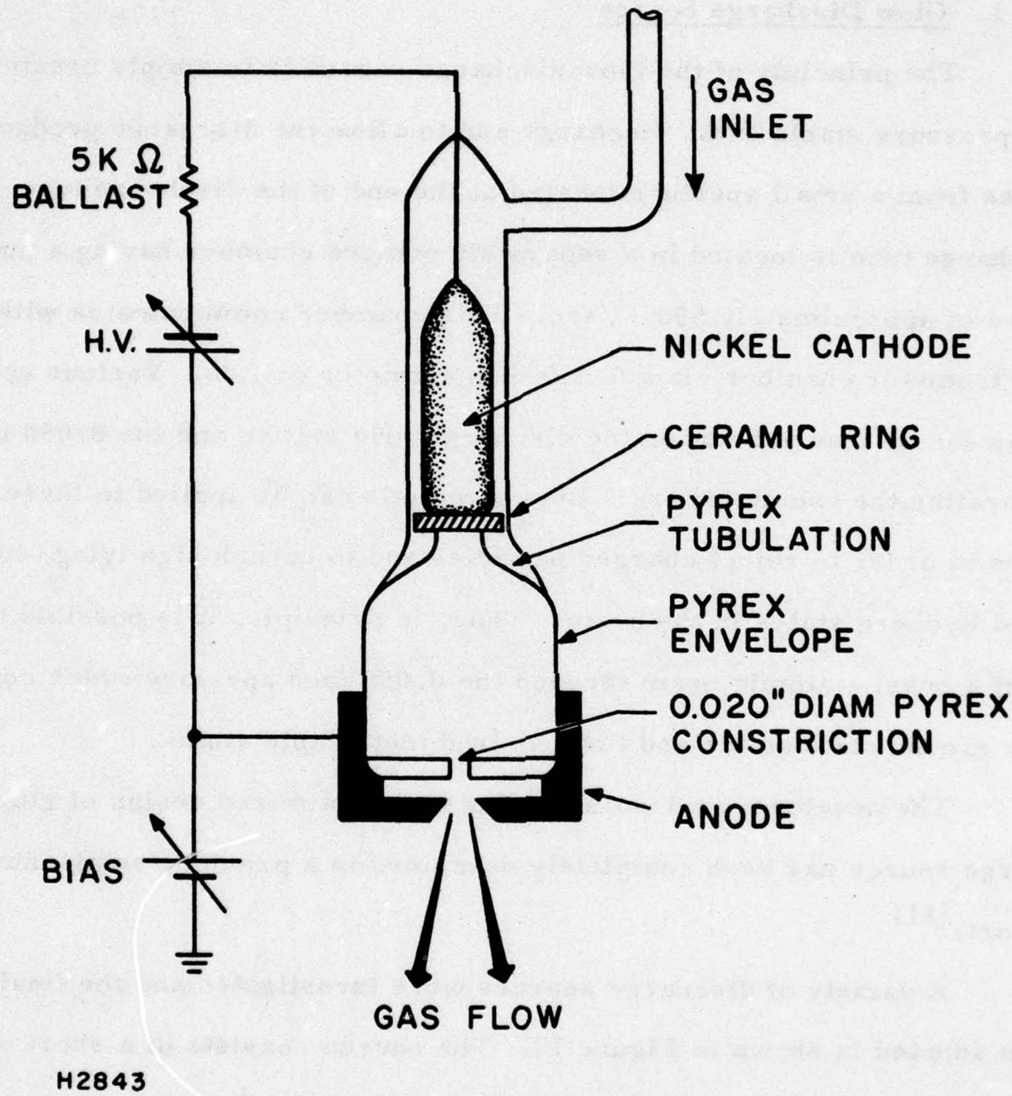

Figure 10 Schematic of the Final Optimized Design of Discharge Tube

The performance of the various sources was assessed by placing an Auger detector approximately 10 cm downstream of the source. The main components of the detector and the operating circuit are shown in Figure 11.

The detector operates on the Auger principle, namely, that metastable atoms possessing excitation energy in excess of the work function of a metal surface may liberate electrons from that metal surface upon impact with it. Usually a highly transparent grid is placed above the metal surface and biased positively with respect to the surface so that the ejected electrons are completely removed. If the secondary emission coefficient for the particular metastable and the particular surface are known then by measuring the current leaving the surface the metastable flux can be estimated. The guard plates ensure high electrical insulation since small currents are normally encountered; the deflector plates are to remove any remaining charged particles from the beam.

Energetic photons may also liberate electrons from the surface of the Auger detector and, therefore, once charged particles have been removed from the beam it is essential to discriminate between the photon and metastable components of the beam both of which contribute to the measured Auger current. The technique adopted for this purpose is due to Stebbings,[14] and is based upon the difference in absorption length of the photon and metastable components of the beam when a background gas is introduced between the source and detector. Much of Stebbings' reported data described the absorption of metastable helium atoms and photons produced in a low pressure

(14) Stebbings, R.F., Proc. Roy. Soc. 241, 270 (1975).

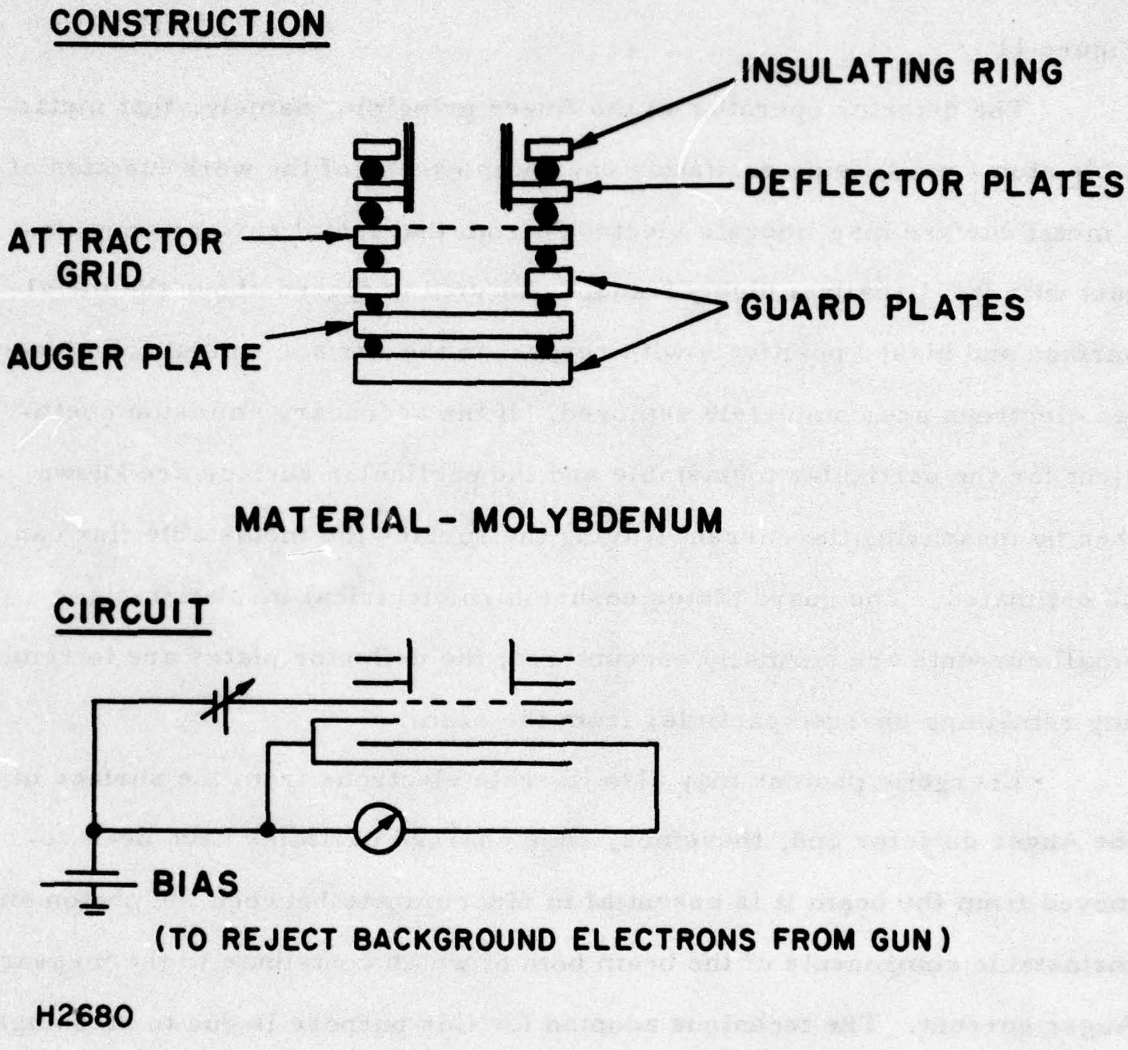

Figure 11 Schematic of the Auger Detector and Operating Circuit

helium discharge by argon gas contained in a gas cell between the source and detector. Therefore, for comparative purposes, the performance of the various discharge tubes was usually determined initially by operating with a helium discharge and performing attenuation measurements of the photon/metastable beam at the Auger detector as a function of argon background gas pressure which could be separately and uniformly introduced into the path of the beam via an auxiliary gas inlet in the spectrometer chamber.

A typical plot of current measured at the Auger detector vs background pressure is shown in Figure 12. This plot is for a helium discharge using argon as the background gas. Two regimes are clearly discernible on the plot, an early rapidly attenuated component followed by a much larger tail. The more slowly decaying component is ascribed to the absorption of photons in the beam which are removed by photoionization of the argon background gas. Since the absorption length is known (10 cm) and the gas pressure is measured, the cross section for this process can be deduced from the slope of the line at higher pressures. The value obtained viz σ 2×10^{-17} cm^2 is in excellent agreement with the value obtained by Stebbings and also by other workers, for the photoionization of argon by helium resonance photons. The photon component can be obtained by extrapolating the long tail of the Auger current to zero pressure. If the photon component is subtracted from the total Auger current and the natural log of the residual current again plotted against background pressure, the cross section for the low pressure process, ascribed to the attenuation of the metastable component can be deduced. Such a plot is shown in Figure 13, the cross section

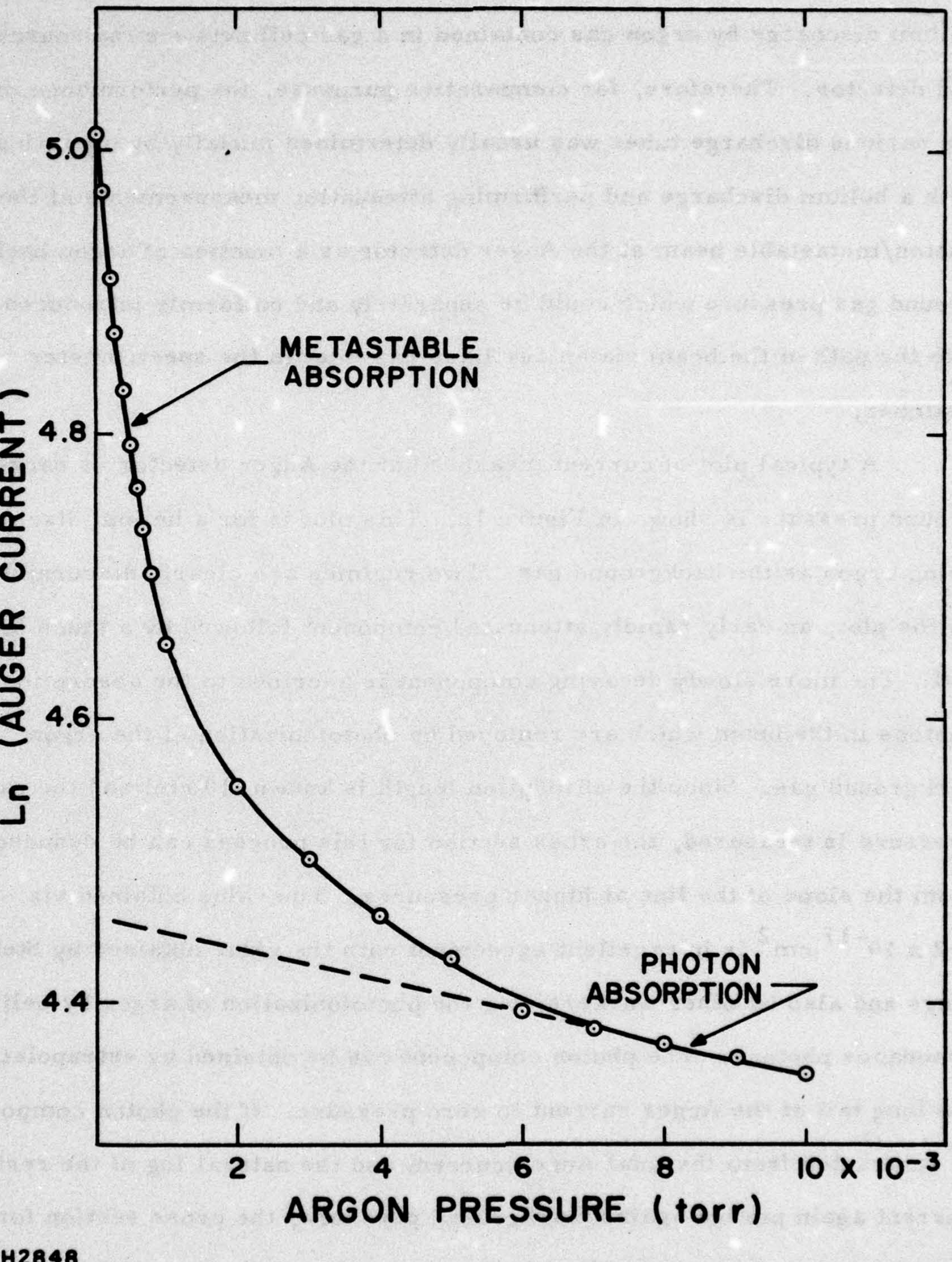

Figure 12 Plot of ℓn Auger Detector Current vs Pressure for a Helium Discharge Using Argon as the Background Gas

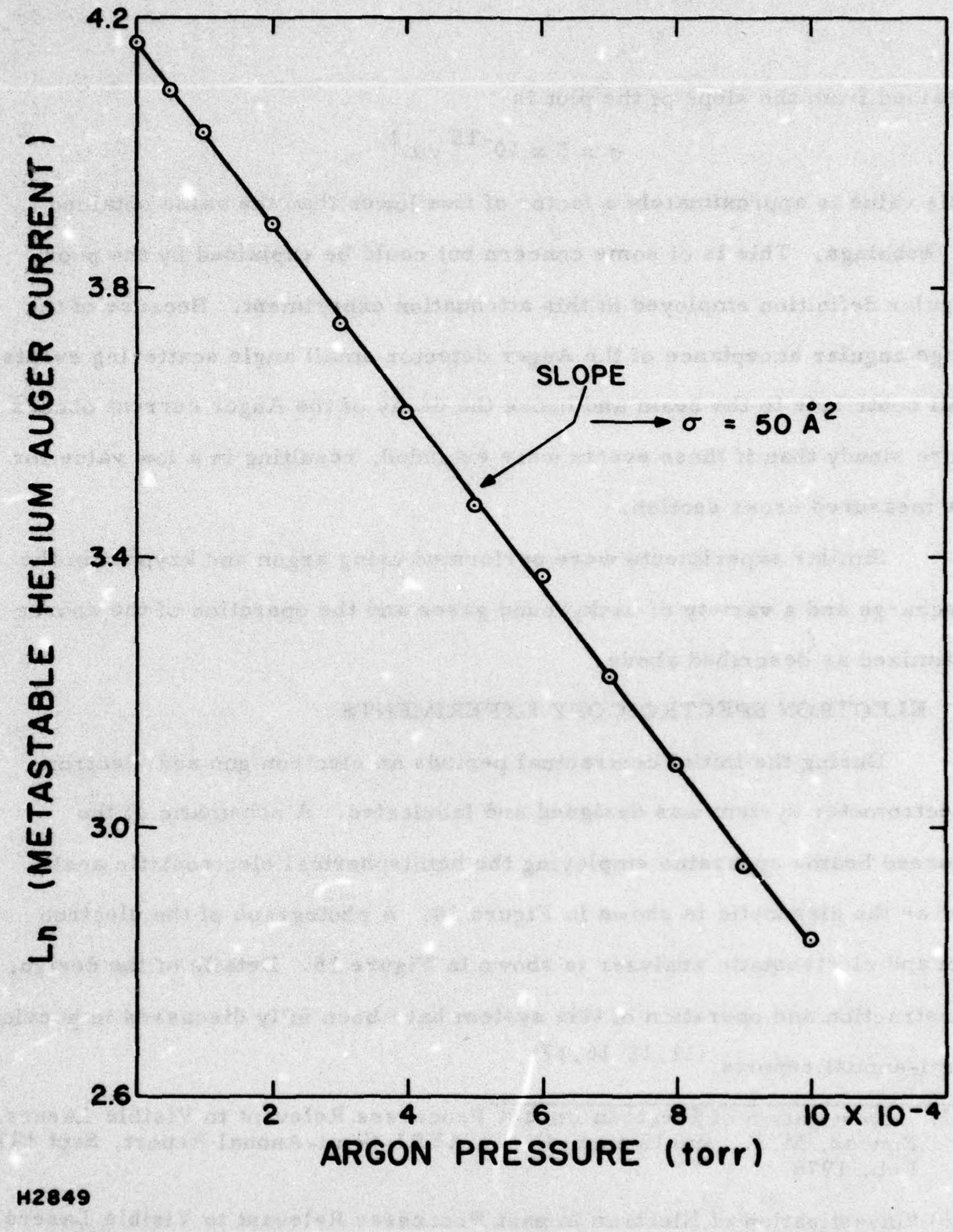

Figure 13 Plot of ℓn Auger Current Minus Photon Components vs Background Pressure

obtained from the slope of the plot is

$$\sigma = 5 \times 10^{-15}\ cm^2$$

This value is approximately a factor of five lower than the value obtained by Stebbings. This is of some concern but could be explained by the poor angular definition employed in this attenuation experiment. Because of the large angular acceptance of the Auger detector small angle scattering events still contribute to the beam and hence the decay of the Auger current occurs more slowly than if these events were excluded, resulting in a low value for the measured cross section.

Similar experiments were performed using argon and krypton in the discharge and a variety of background gases and the operation of the source optimized as described above.

C. ELECTRON SPECTROSCOPY EXPERIMENTS

During the initial contractual periods an electron gun and electron spectrometer system was designed and fabricated. A schematic of the crossed beams apparatus employing the hemispherical electrostatic analyzer as the diagnostic is shown in Figure 14. A photograph of the electron gun and electrostatic analyzer is shown in Figure 15. Details of the design, construction and operation of this system have been fully discussed in previous semi-annual reports.[11,15,16,17]

---

(15) "Investigation of Electron Impact Processes Relevant to Visible Lasers." Boness, M.J., and Hyman, H.A., AERL Semi-Annual Report, Sept 1975-Feb. 1976.

(16) "Investigation of Electron Impact Processes Relevant to Visible Lasers." Boness, M.J., and Hyman, H.A., AERL Semi-Annual Report, March 1976-Aug. 1976.

(17) "Investigation of Electron Impact Processes Relevant to Visible Lasers." Boness, M.J., and Hyman, H.A., AERL Semi-Annual Report, Sept. 1976-Feb. 1977.

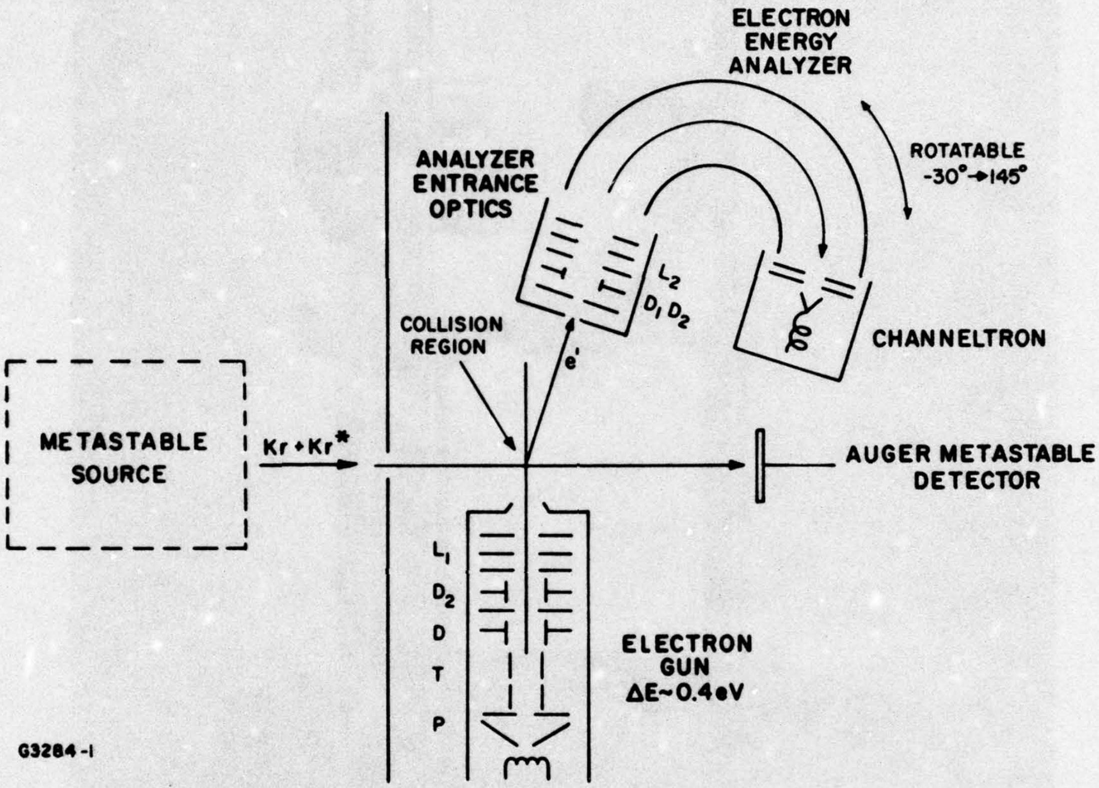

Figure 14 Schematic of the Crossed Beams Apparatus for Electron Scattering from Metastable States of Rare Gases

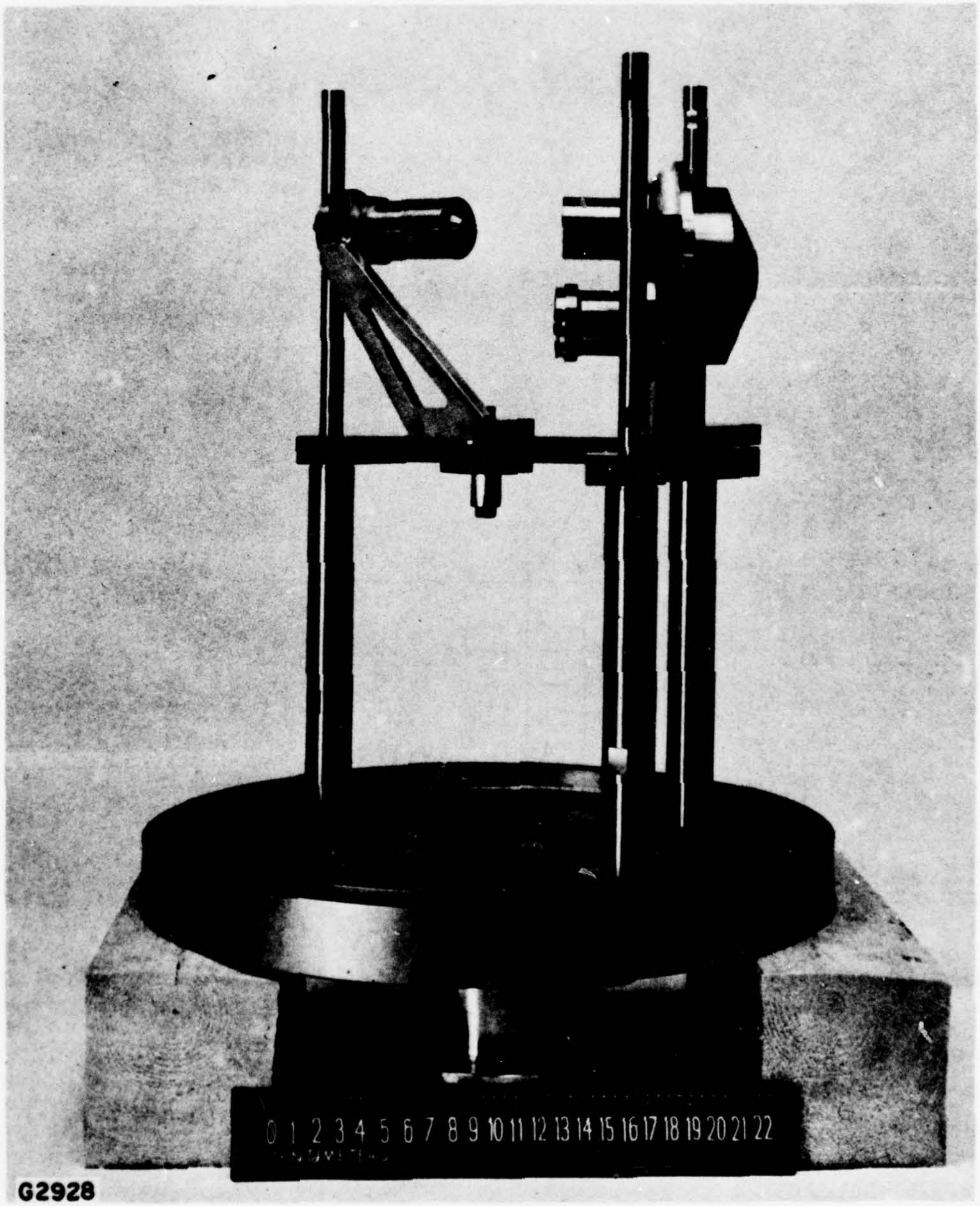

Figure 15 Photograph of Electron Gun and Hemispherical Electrostatic Analyzer Mounted on Wheeler Flange

Operating the glow discharge with argon, experiments were performed according to the original conception of the measurement. Over the angular range accessible to the experiment and at a variety of incident electron energies no measurable electron-metastable scattering energy loss signals in the vicinity of 1.6 eV corresponding to the transition

$$\text{Ar}\ (4sj) + e \rightarrow \text{Ar}\ (4pj') + e$$

were detected.

This transition is, of course, a strongly allowed optical transition. It is well known that at <u>high</u> electron energies angular distributions for the scattered electrons are strongly peaked in the forward direction. At low energies generalizations are more difficult and several factors such as resonance phenomena and the limited number of partial wave contributions to the scattering amplitude complicate the issue tremendously. Thus the non-isotropic behavior of the angular distribution combined with the signal-to-noise limitations imposed by spurious scattering signals and long term stability which limited the signal averaging periods could be a valid explanation for the absence of the scattered electron signal over the angular range accessible to the experiment.

D. THE FLUORESCENCE TECHNIQUE

Due to the problems encountered with the technique of energy loss spectroscopy the possibility of a fluorescence measurement was considered as a method of observing the process of interest,

$$\text{viz}\quad e + \text{Kr}^*\ (5sj) \rightarrow \text{Kr}^{**}\ (5pj') + e$$

via the fluorescence

$$\text{Kr}^{**}\ (5pj') \rightarrow \text{Kr}\ (5sj) + h\nu$$

A comparison of the relative sensitivities of the fluorescence technique and the method of energy loss spectroscopy involves many factors. The near isotropic nature of the fluorescence emission together with the possibility of employing large f-number extraction optics strongly favors the fluorescence technique. However, detector sensitivity, intrinsic noise, and spectrometer transmission efficiency favor energy loss spectroscopy. After considering each of these factors it appeared that the fluorescence technique might provide a better opportunity to perform this particular measurement.

An additional benefit accrued from adopting the fluorescence technique was the possibility to increase the incident e-beam intensity by using larger apertures in the diode stage of the gun. This improvement was not possible when employing the electron spectrometer since the corresponding increase in the angular divergence and space charge spreading of the e-beam significantly reduced the signal-to-noise ratio due to a very large increase in electron scattering signals from surfaces.

Once the decision was taken to adopt the fluorescence technique the experiment was modified accordingly. A schematic of the fluorescence diagnostic arrangement is shown in Figure 16. Rather than employ an optical extraction system comprised of lenses which requires careful alignment, a light pipe system was employed as shown. The light pipe was 3/8 inch diameter quartz and subtended approximately an f1 ratio at the collision region. The light pipe was sealed through the wall of the vacuum chamber using a viton o-ring seal. A stainless steel bellows arrangement was employed for alignment purposes. The end of the light pipe was focussed onto the entrance slit of a 1/4-meter Jarrel-Ash monochromator using

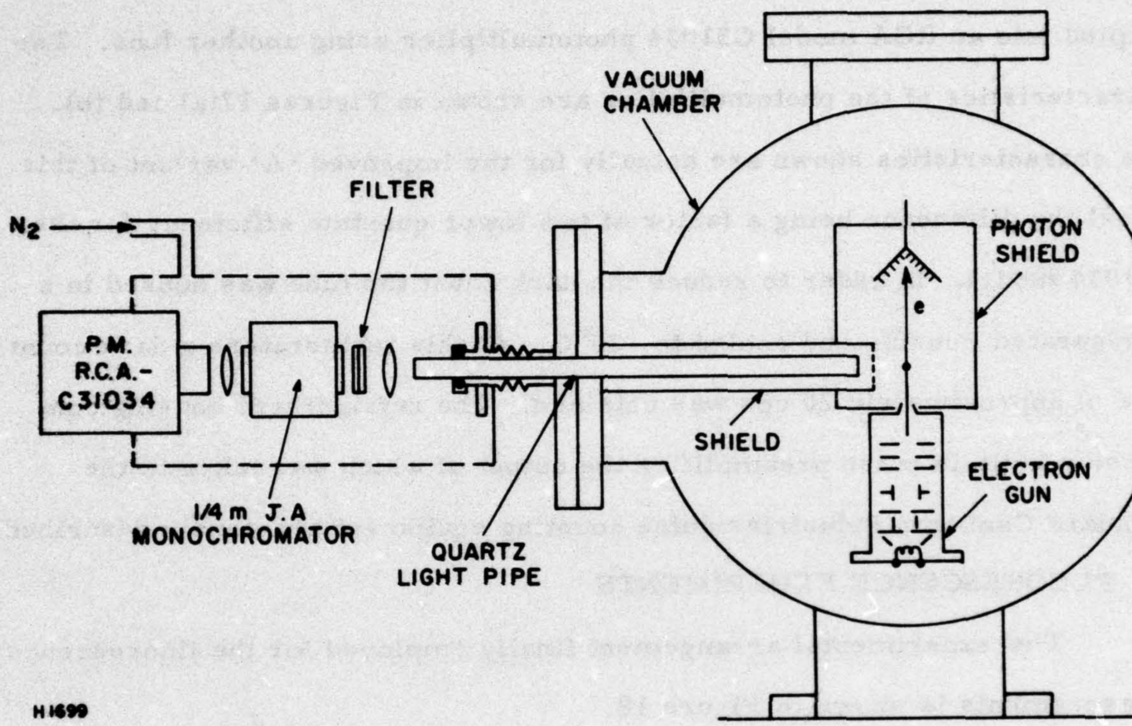

Figure 16 Schematic of the Fluorescence Diagnostic Arrangement

a cylindrical lens. A blocking filter which defined the spectral region of interest was interposed between the cylindrical lens and the entrance slit of the monochromator. The monochromator was equipped with a 590 lines/mm grating blazed at 750 nm. The exit slit of the monochromator was coupled into an RCA model C31034 photomultiplier using another lens. The characteristics of the photomultiplier are shown in Figures 17(a) and (b). The characteristics shown are actually for the improved 'A' variant of this model the difference being a factor of two lower quantum efficiency for the C31034 model. In order to reduce the dark count the tube was housed in a refrigerated housing and cooled to $-20^{o}C$. At this temperature a dark count rate of approximately 20 cps was obtained. The refrigerated housing contained a built-in pulse preamplifier the output of which was taken to the standard Canberra Industries pulse counting equipment previously described.

E. FLUORESCENCE EXPERIMENTS

The experimental arrangement finally employed for the fluorescence measurements is shown in Figure 18.

As with the energy loss spectroscopy considerable problems were encountered with background noise signals originating in the experiment itself. The photon background generated by the discharge overlapped exactly the fluorescence signals of interest and was extremely difficult to cope with. The signal was reduced as much as possible by introducing a complete shield around the collision region as shown and by collecting the major component of the photon flux inside the Woods' Horn which was open at the small end in order to vent the box.

Photons emitted from the filament which travelled collinearly through the collision region with the e-beam and then scattered off various surfaces

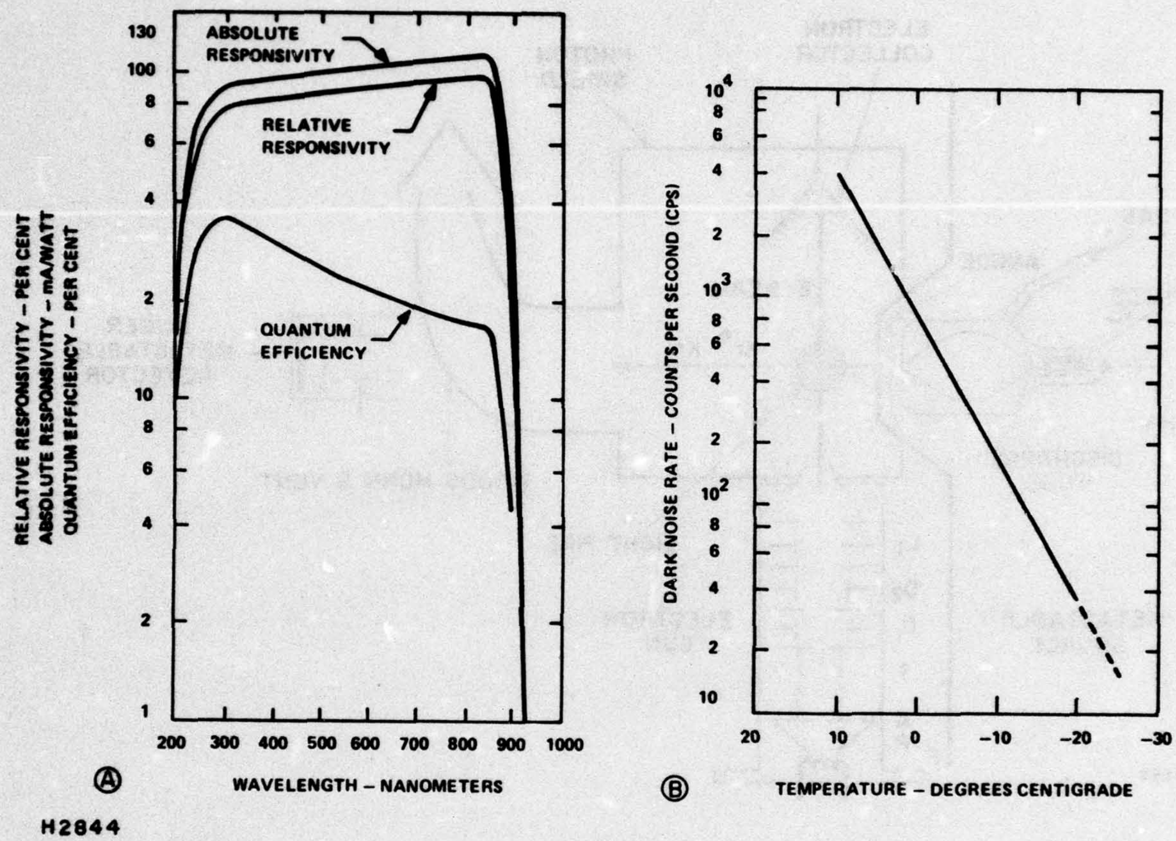

Figure 17 (a) Typical Photocathode Spectral Responsivity Characteristics of the RCA Model C31034A Photomultiplier

(b) Typical Dark Noise Rate as a Function of Temperature

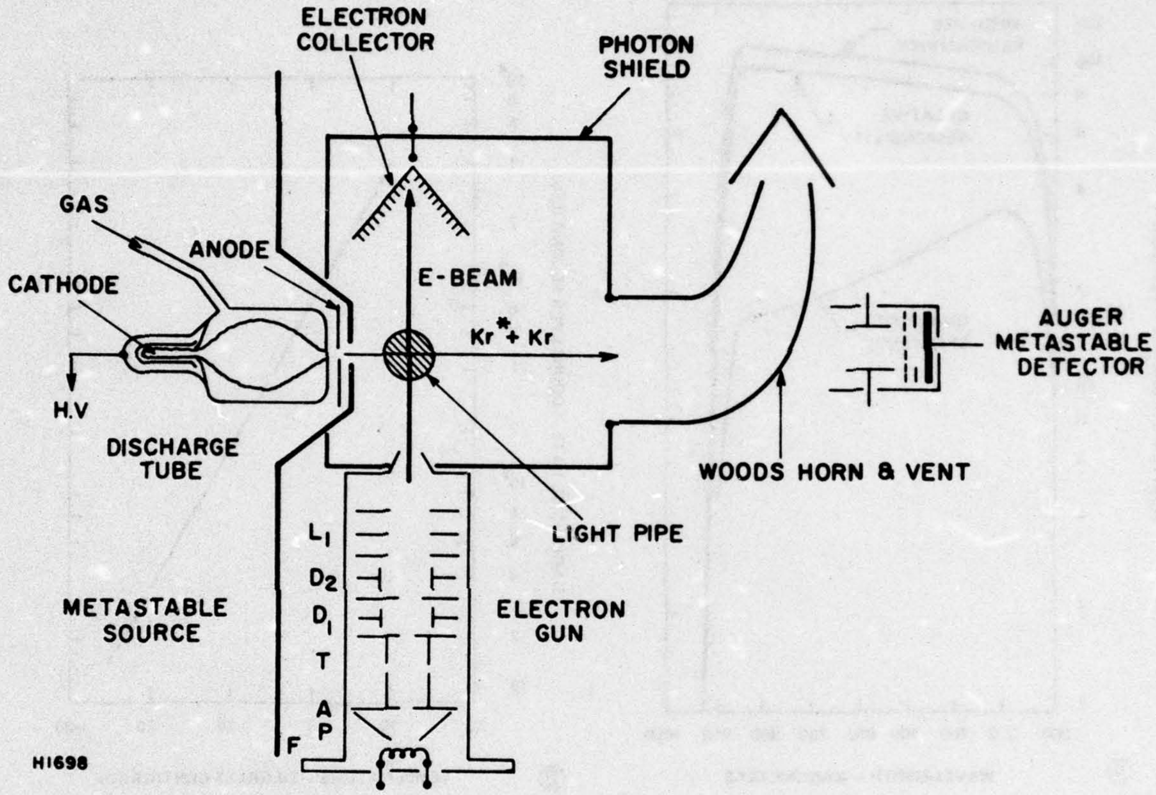

Figure 18 Schematic of the Experimental Arrangement Employed for the Fluorescence Measurement

into the collection optics were another problem. This was reduced considerably by providing the venetian blind style electron collector which both monitored the primary e-beam and provided a dump for the continuum emission from the filament.

Initially experiments were performed to measure the Ar (4pj') → Ar (4sj), Kr (5pj') → Kr (5sj) and Xe (6pj') → Xe (6 sj), fluorescence by exciting the npj' levels directly by electron collisions with ground state atoms. This served to verify the performance of the system and also to provide a convenient method of exactly calibrating the monochromator reading for the wavelengths of interest. Naturally, the discharge was unnecessary for these experiments; the primary e-beam was simply crossed with a beam of ground-state atoms. Fluorescence spectra for the transitions of interest in argon, krypton and xenon obtained at an incident electron energy of approximately 20 eV are shown in Figures 19-21, respectively.

1. Metastable Scattering Experiments

Since the electron-metastable induced fluorescence signals never exceeded 1% of the background fluorescence noise signal long term signal averaging procedures were routinely employed with accumulation periods typically averaging 1-2 x 10^3 sec. In practice, the discharge and electron gun were operated for several hours prior to data accumulation to ensure complete outgassing of the discharge electrodes, thermal stability in the electron gun, stabilization of the background pressure and electron gun emission current.

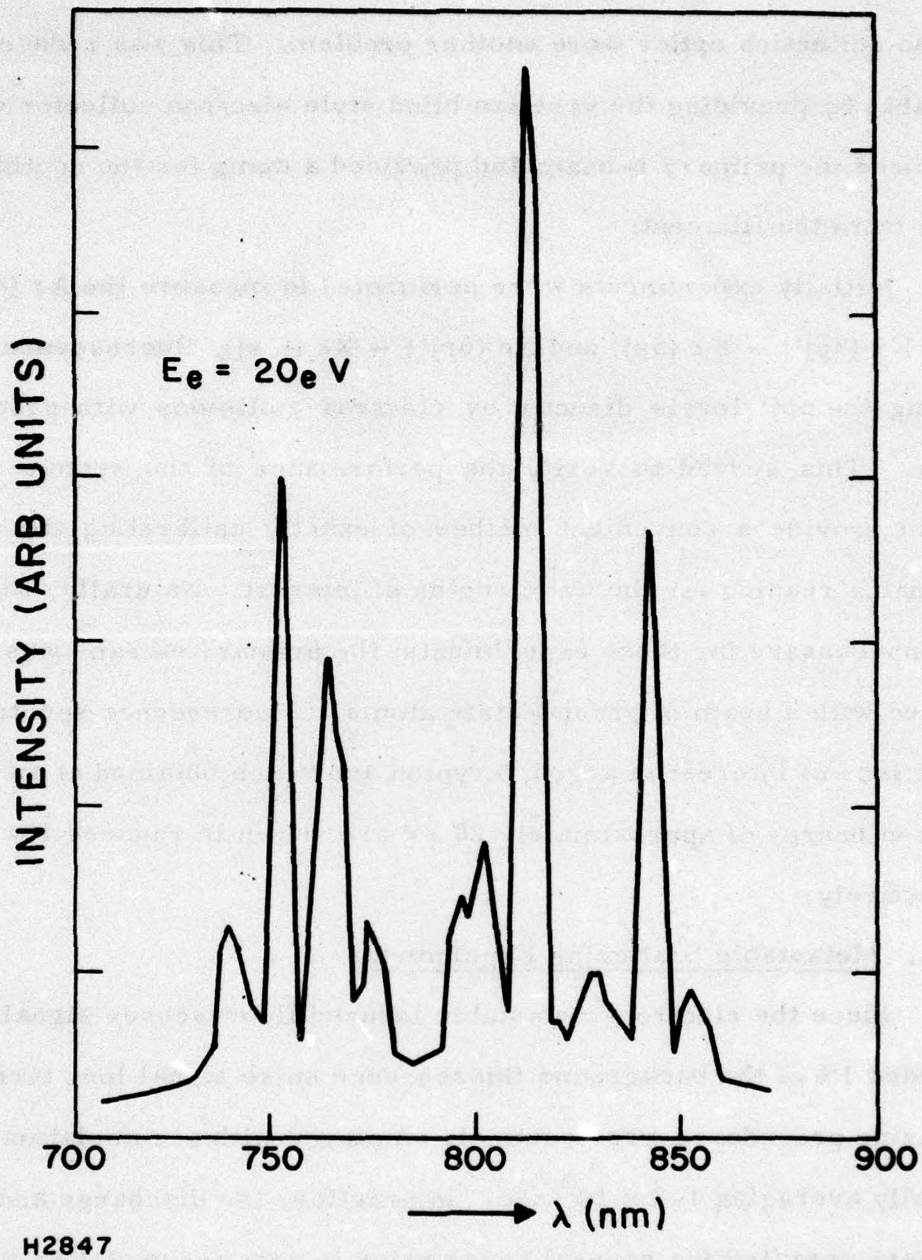

Figure 19 Fluorescence Spectrum for the Argon Ar (4pj') → Ar (4sj) Transitions Obtained at an Electron Energy of 20 eV

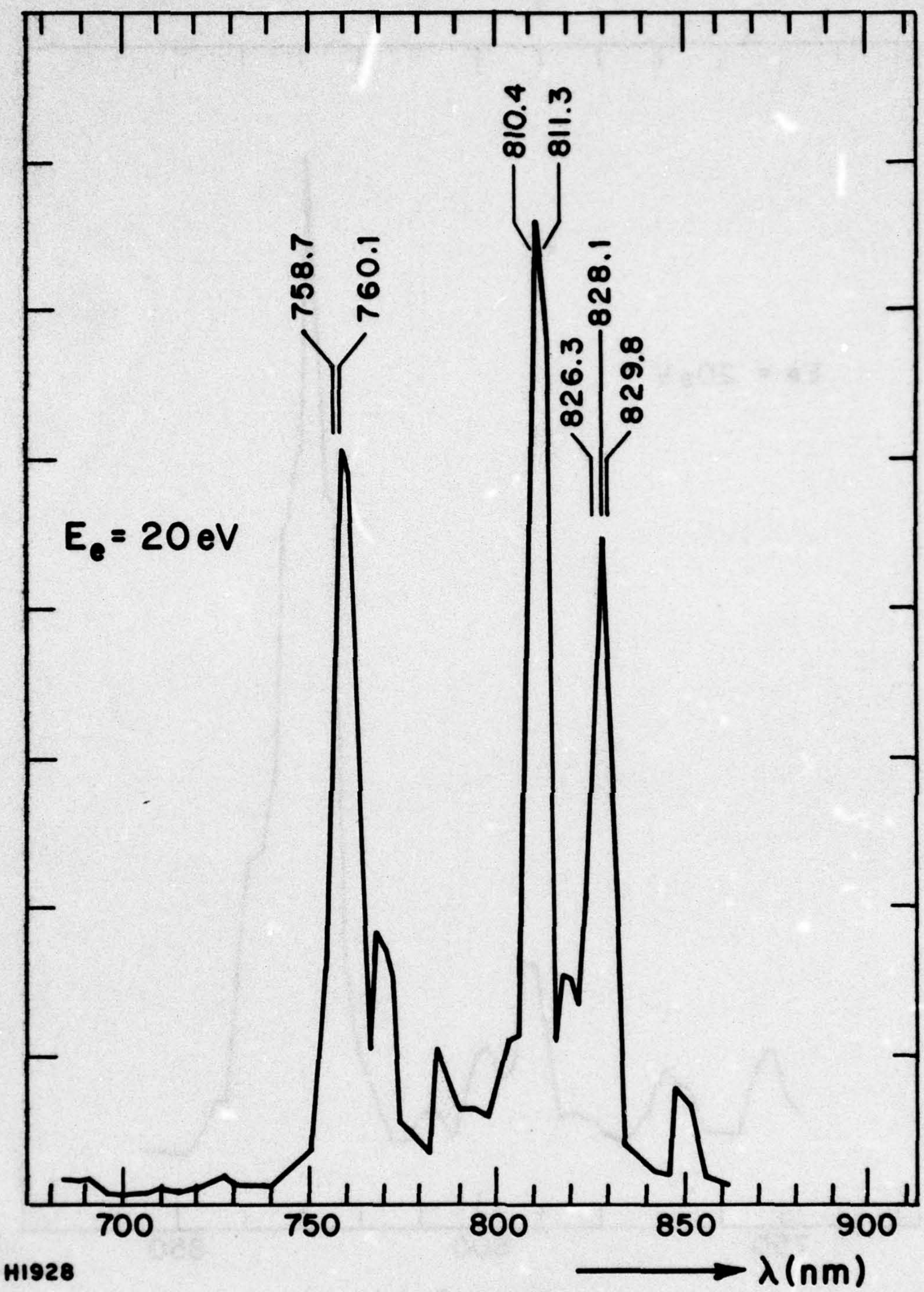

Figure 20 **Fluorescence Spectra for the Krypton Kr (5pj') → Kr (5pj) Transitions Obtained at an Electron Energy of 20 eV**

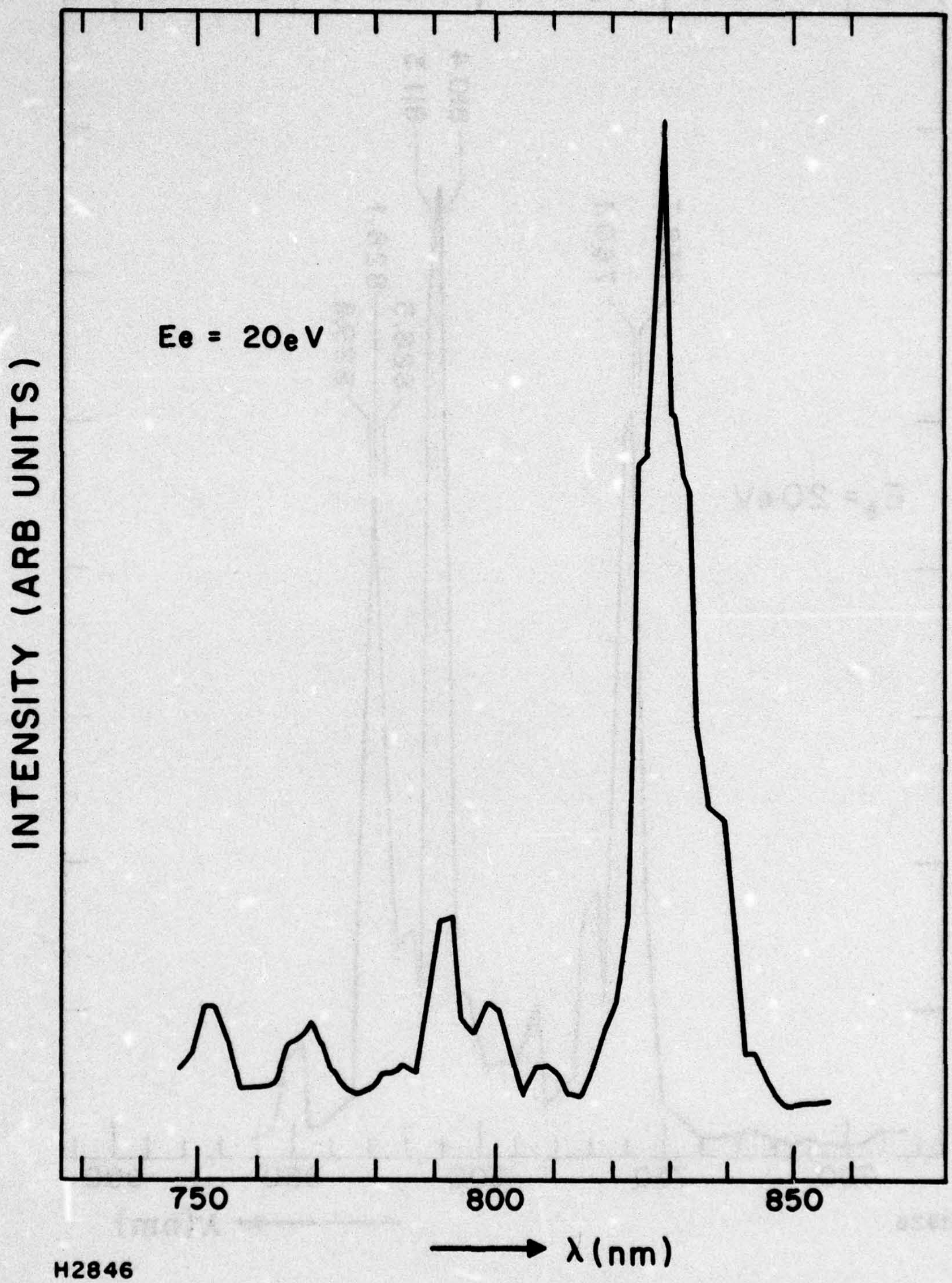

Figure 21 **Fluorescence Spectrum for the Xe (6pj') → Xe (6sj) Transitions Obtained at an Electron Energy of 20 eV**

Data accumulation was performed by selecting the wavelength of interest in the 1/4 meter monochromator and then adjusting the e-beam energy to the required value. The electron-metastable fluorescence signal was detected as the difference between the signals collected with the e-beam on and off. Rather than modulate the e-beam by reducing the heater current which would also have slightly modulated the photon noise background due to filament emission the voltages applied to the electron gun were reduced to zero. At e-beam energies significantly lower than the energy required to excite the upper fluorescing level directly from the ground state the difference signal corresponded to fluorescence from electron-meatastable collisions. However, since the ratio of metastable to ground-state species in the beam was extremely small spurious signals could, in principle, occur due to the high energy tail of the e-beam distribution (although orders of magnitude less than the peak intensity) interacting directly with ground-state species. In practice, such signals were detected by repeating the e-beam "on" and "off" experiments with the discharge tube off but maintaining the gas flow. Such signals were only detected when the nominal e-beam energy was within a volt of the threshold energy for direct excitation from the ground state.

Measurements were attempted at wavelengths corresponding to the various peaks in the fluorescence spectra shown in Figures 19-21, however the very large background photon flux, extraneous noise problems and limits to long term stability of operation interfered considerably with data accumulation. Data corresponding to fluorescence from electron-metastable and electron-ground state collisions is presented in Figures 22-25. For krypton reliable electron-metastable collision signals over an extended energy

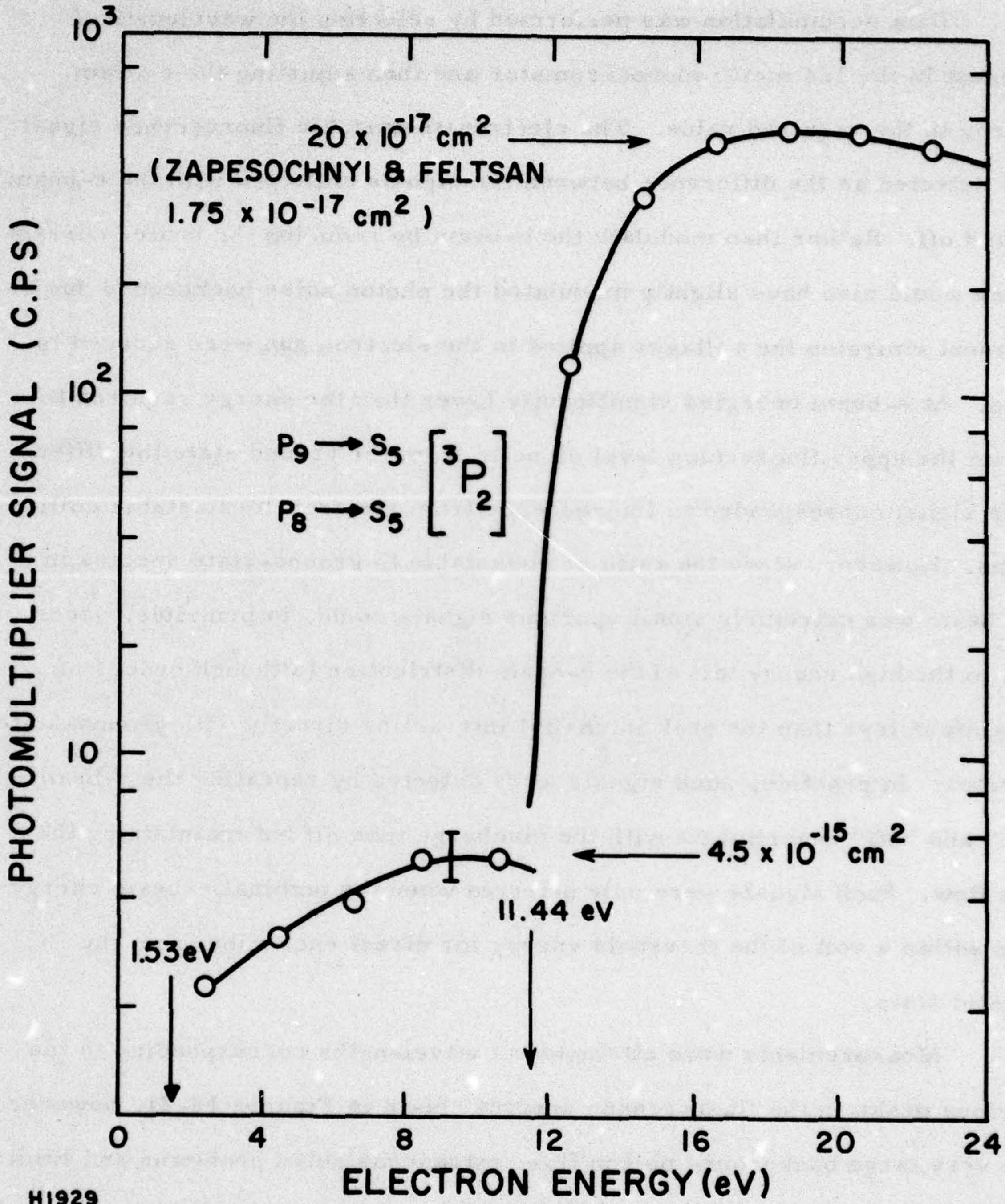

Figure 22 **Energy Dependence of the Combined Line Excitation Signal for the 8104 Å $p_9 \rightarrow s_5$ and 8113 Å $p_8 \rightarrow s_5$ Transitions in Krypton**

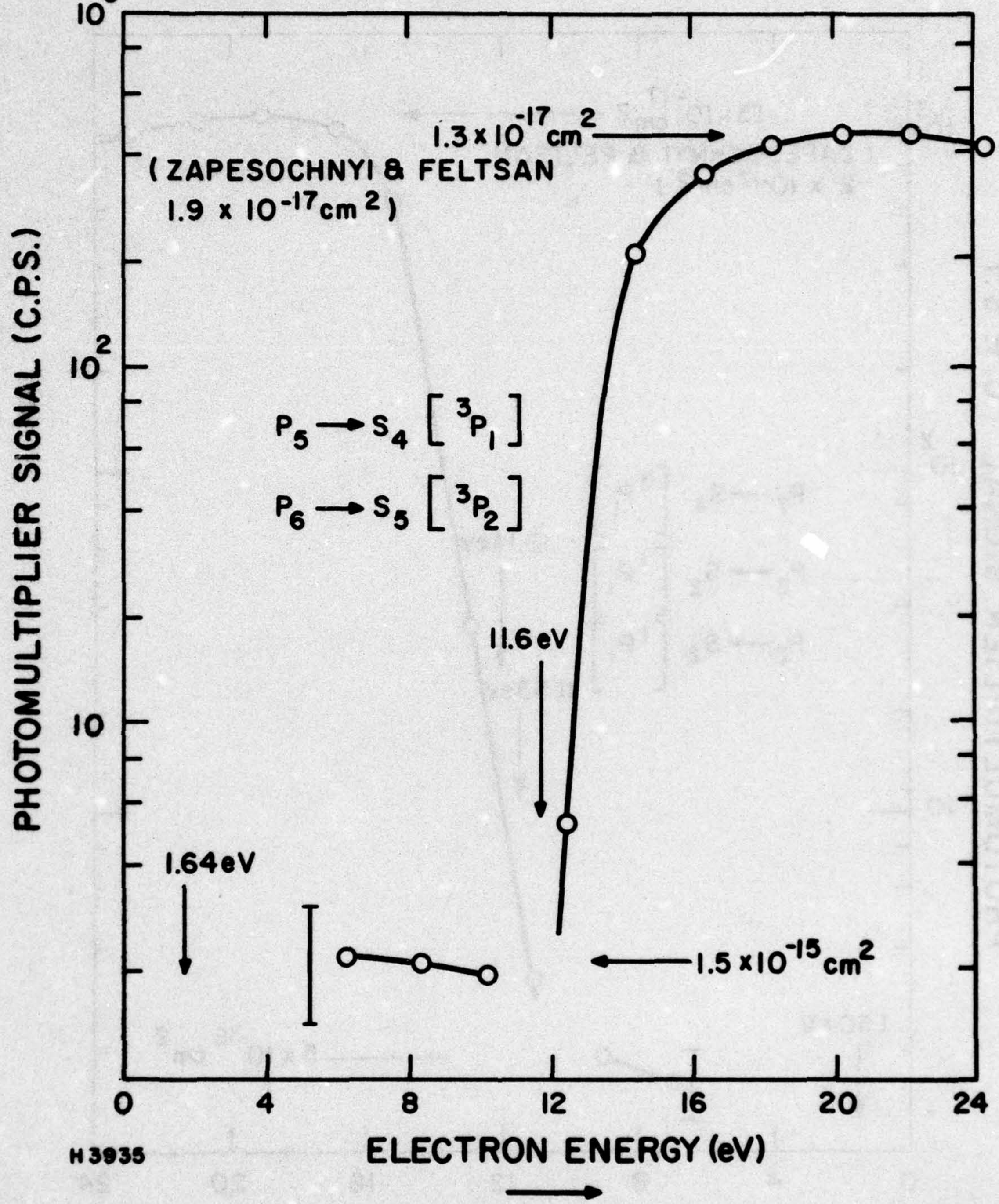

Figure 23 Energy Dependence of the Combined Line Excitation Signal for the 7587 Å $p_5 \rightarrow s_4$ and 7602 Å $p_6 \rightarrow s_5$ Transitions in Krypton

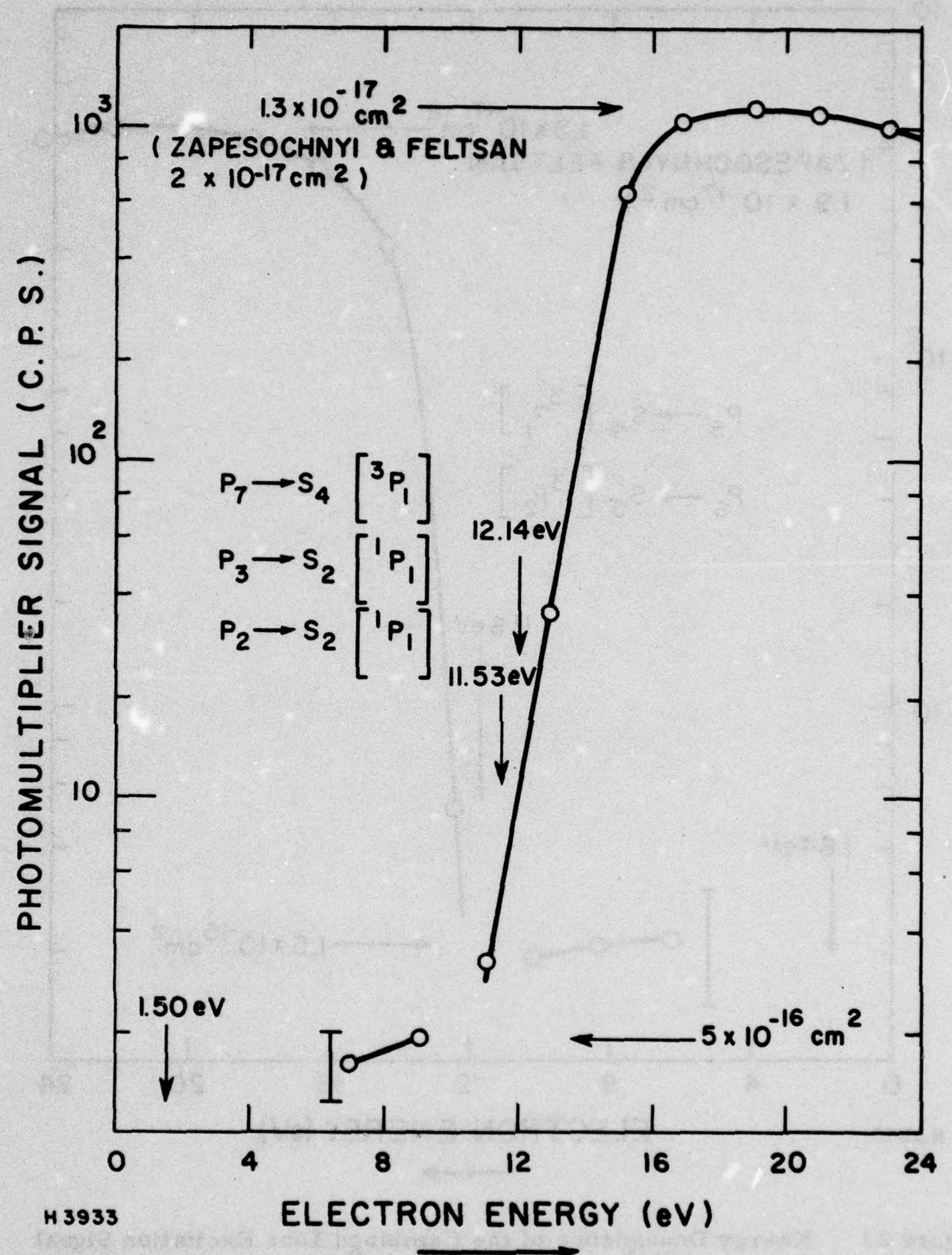

Figure 24 Energy Dependence of the Combined Line Excitation Signal for the 8263 Å $p_7 \rightarrow s_4$, 8281 Å $p_3 \rightarrow s_2$ and 8298 Å $p_2 \rightarrow s_2$ Transitions in Krypton

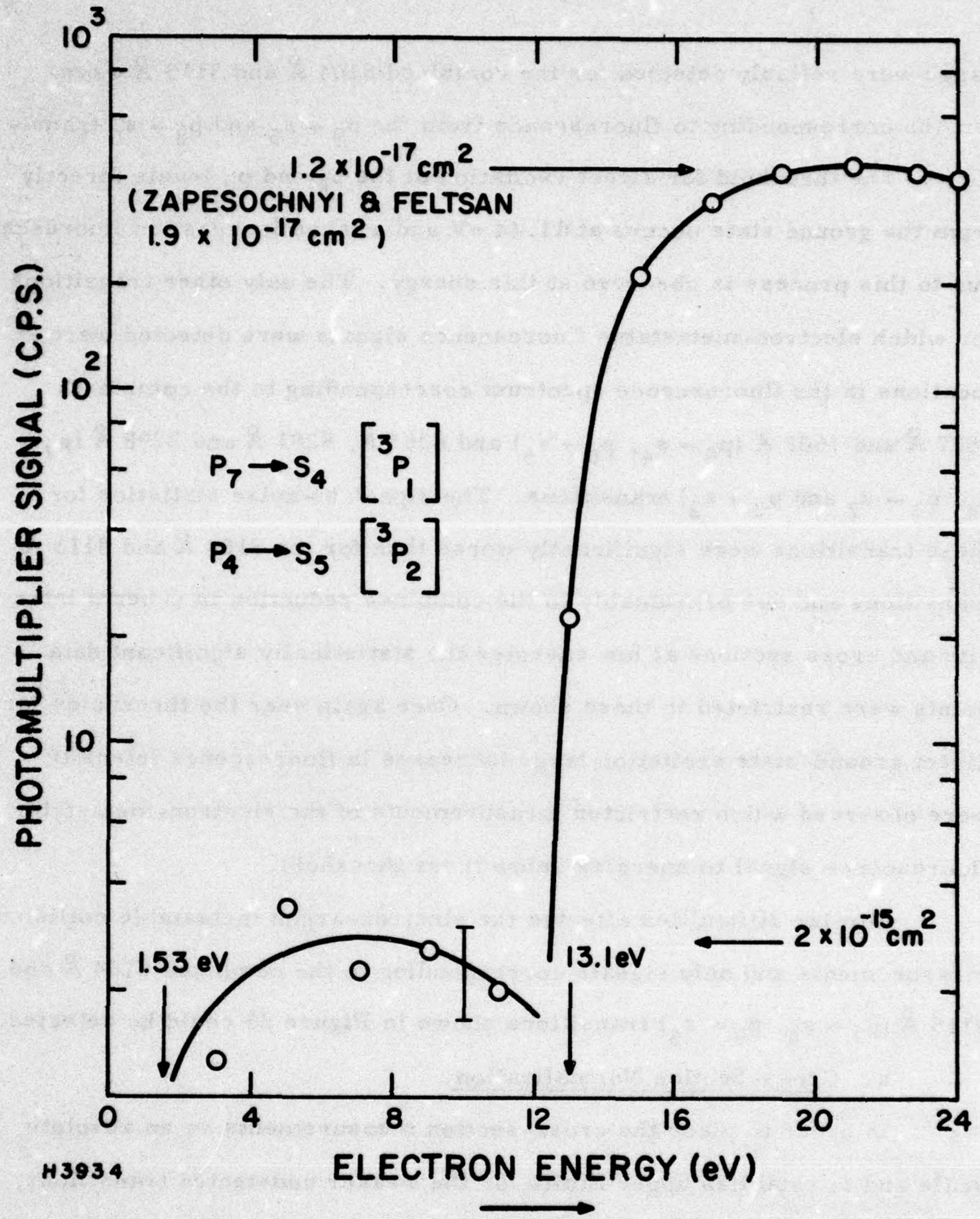

Figure 25 Energy Dependence of the Combined Line Excitation Signal for the 8104 Å $p_7 \rightarrow s_4$ and 8115 Å $p_9 \rightarrow s_5$ Transitions in Argon

range were reliably detected for the combined 8104 Å and 8113 Å wavelengths corresponding to fluorescence from the $p_9 \rightarrow s_5$ and $p_8 \rightarrow s_5$ transitions. The threshold for direct excitation of the p_8 and p_9 levels directly from the ground state occurs at 11.44 eV and a large increase in fluorescence due to this process is observed at this energy. The only other transitions for which electron-metastable fluorescence signals were detected were at locations in the fluorescence spectrum corresponding to the combined 7587 Å and 7602 Å ($p_5 \rightarrow s_4$, $p_6 \rightarrow s_5$) and 8263 Å, 8281 Å and 8298 Å ($p_7 \rightarrow s_4$, $p_3 \rightarrow s_2$ and $p_2 \rightarrow s_2$) transitions. The signal-to-noise statistics for these transitions were significantly worse than for the 8104 Å and 8113 Å transitions and due presumably to the combined reduction in e-beam intensity and cross sections at low energies the statistically significant data points were restricted to those shown. Once again near the thresholds for direct ground-state excitation large increases in fluorescence intensity were observed which restricted measurements of the electron-metastable fluorescence signal to energies below these threshold.

Similar difficulties affected the electron-argon metastable collision measurements and only signals corresponding to the combined 8104 Å and 8115 Å ($p_7 \rightarrow s_4$, $p_9 \rightarrow s_5$) transitions shown in Figure 25 could be detected.

a. Cross-Section Normalization

In order to place the cross-section measurements on an absolute scale and to establish upper limits for the weaker undetected transitions, the following normalization procedure was adopted. First, the direct ground-state excitation cross section for the transition of interest was normalized with respect to the He 7065 Å $3^3S \rightarrow 2^3P$. This cross section has been measured absolutely by a number of authors and good agreement exists between the various measurements. This transition was selected because it falls within the spectral range occupied by the transitions of interest in krypton and argon and therefore does not introduce additional uncertainties due to variations in the spectral response of the photomultiplier. The value of

$$\sigma = 1.1 \times 10^{-18} \text{ cm}^2$$

for the peak cross section obtained by Jobe & St. John,[18] and which occurs close to threshold was employed for the normalization. The energy dependence of the He $S^3 \rightarrow 2^3P$ clearly indicating the resonant nature of the threshold behavior is shown in Figure 26. Absolute measurements of the ground state line excitation cross sections have been made by Zapesochnyi and Feltsan,[19] however normalization of the present measurements via the helium excitation function was preferred since the helium data has been substantiated within 20% by three independent groups of authors and, therefore, provided a more reliable basis for the normalization. It also provides a basis for comparison with the Zapesochnyi & Feltsan data and which is indicated on Figures 22-25. Since the published data includes all transitions from the various p states to all final s states excluding the ground state, these cross sections had to be adjusted according to the appropriate ratio of oscillator strength to account for those transitions not included in the present measurements. For this purpose the appropriate transition probabilities recently calculated by Lilly[20] were employed.

(18) Jobe, J.D. & St. John, R.H., Phys. Rev. 164, 117-121 (1967).

(19) Zapesochnyi, I.P. and Feltsan, P.V., Optika i Spectrosk (USSR), 20, 521 (1966) English translation in: Optics & Spectrosc (USA) 20, 291 (1966).

(20) Lilly, R.A., J.Opt. Soc. Am. 66, 245 (1976).

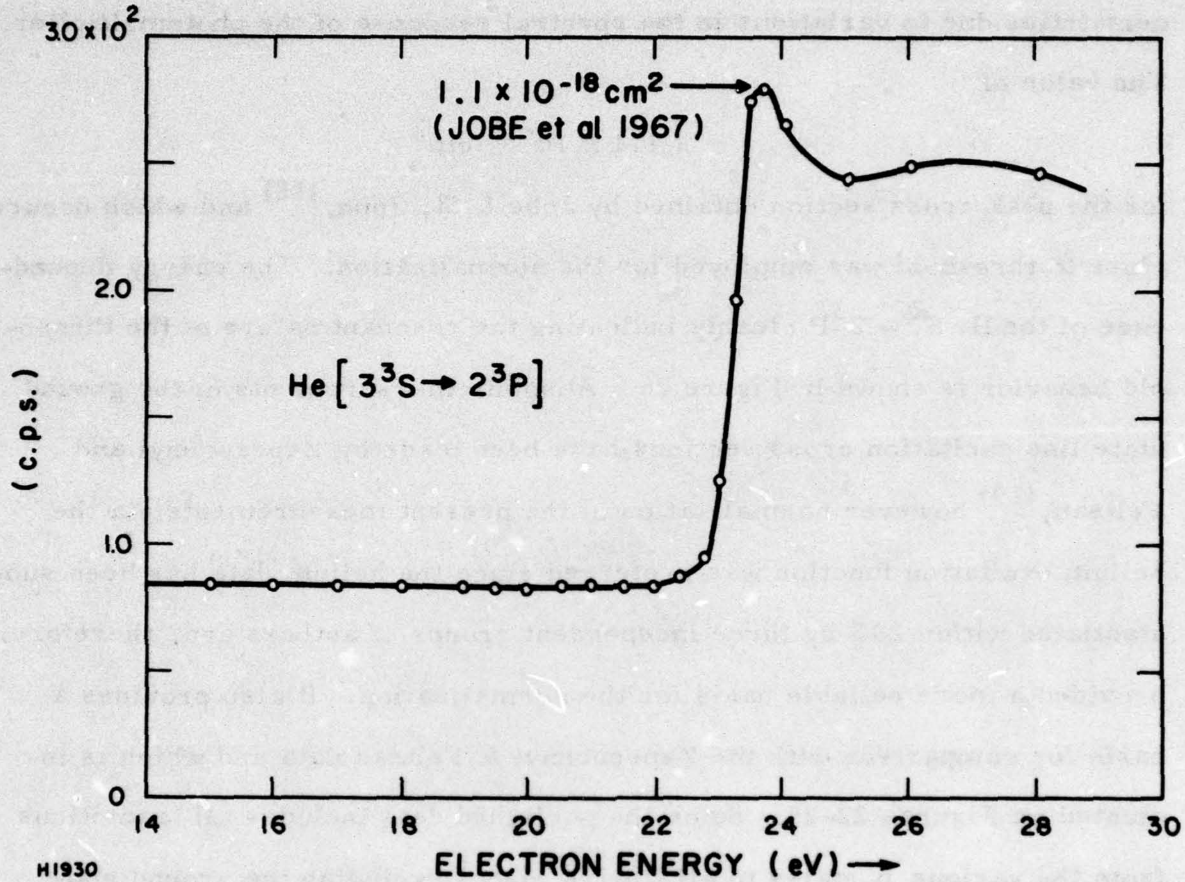

Figure 26 **Energy Dependence for the He $3^3S \rightarrow 2^3P$ Transition at λ = 7065 Å**

Finally, in order to place the electron-metastable line excitation cross sections on an absolute scale, it was necessary to determine the ratio of metastable to ground-state species in the atomic beam.

Knowing the secondary electron emission coefficient (γ) for the metastable species in question on the surface of the Auger detector, then absolute metastable densities at the detector location could be determined from the magnitude of the metastable component of the Auger current deduced from attenuation measurements similar to that shown in Figure 12. This value was extrapolated back to obtain the absolute value of the metastable density at the collision region defined by the interception of the electron and atomic beams.

The value of γ for argon metastables incident on a gold plated surface ($\gamma = 0.5$) was taken from the work of Dunning et al.,[21] the value of γ used for krypton was 0.25.

The absolute value of the ground-state atom density at the collision was determined from measurements performed with the electrostatic electron energy analyzer system described in Section II.C.

As previously described for the electron spectroscopy experiments the collision volume defined by the acceptance angle of the electrostatic analyzer acceptance optics was designed to be invariant with respect to angular location as illustrated in Figure 27 in order to provide accurate relative angular distribution measurements. For purposes of determining the ground-state atom density (performing the fluorescence measurements) the angular divergence of the atomic beam was increased so that the cross-

(21) Dunning, F.B., Rundel, R.D., Stebbing, R.F. Rev. Sci. Inst. 46, 697 1975.

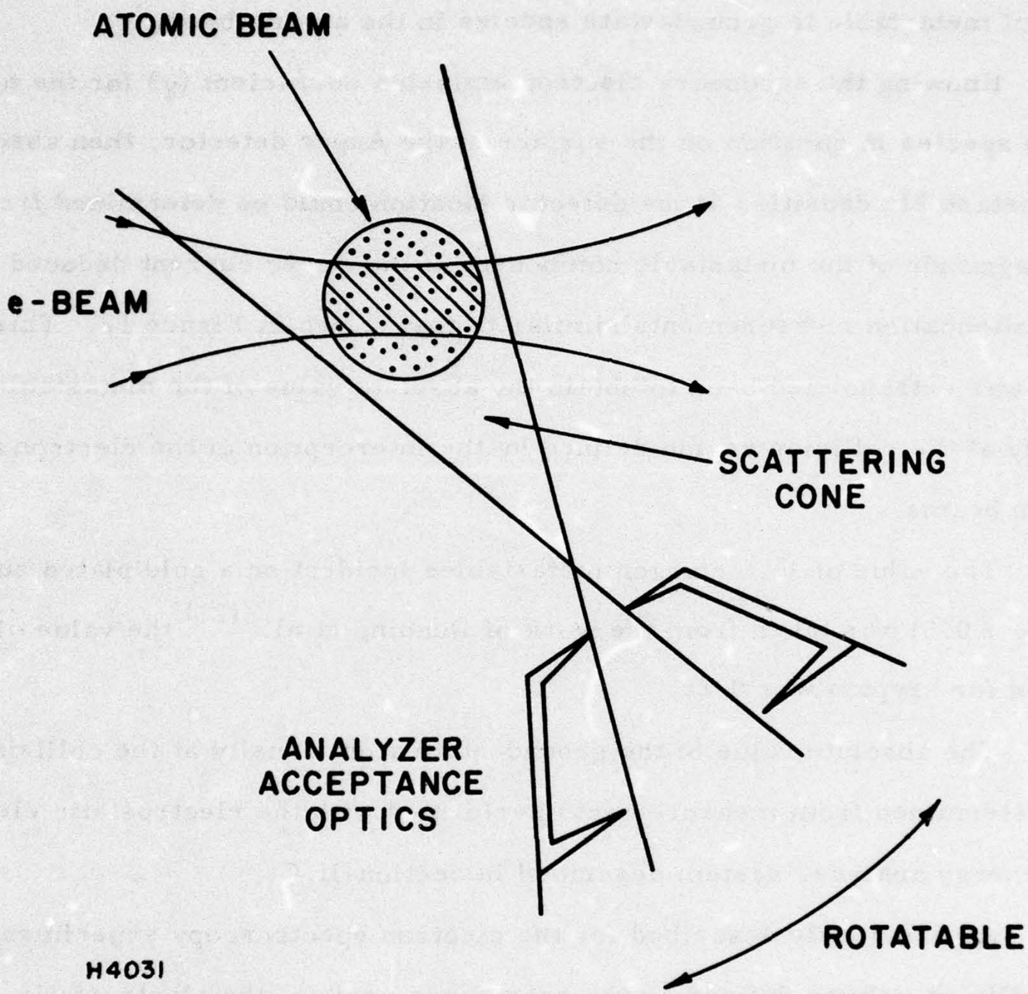

Figure 27 Diagram of the Collision Chamber Geometry Employed for the Electron Spectroscopy Experiments

sectional area exceeded the area intercepted by the acceptance angle defined by the electrostatic analyzer acceptance optics and the e-beam for 90° scattering as shown in Figure 28.

Using this geometry the metastable source gas flow rate was adjusted to yield the usual optimized background pressure conditions and the elastic electron scattering signal through the electrostatic analyzer as measured by the channeltron count rate was measured. The atomic beam was then turned off and gas introduced into the spectrometer chamber through a separate large diameter (3/4") orifice remote from the collision region until the scattering signal measured by the channeltron count rate was equal to that obtained with the atomic beam operating. Under the latter conditions the pressure is uniform throughout the chamber and was measured on the ion gauge. Since the collision volume is invariant under the two conditions as illustrated by comparing Figures 28(a) and 28(b), then the background pressure measurement determines the atomic beam density and, thus, yields the absolute value of the ground-state atom density required to provide the ratio of metastable-to-ground state densities necessary for the metastable cross-section normalization procedure.

The values of the metastable excitation cross sections are indicated in Figures 22-25. The vertical bar on the figures indicates one standard deviation for the statistical variation imposed by the background signal counting rate and represents the statistical accuracy to which the metastable scattering signal could be determined. Incomplete suppression of extraneous signal interference would reduce the accuracy determined by statistical fluctuations. These interferences were rountinely & periodically verified to be absent during data accumulation.

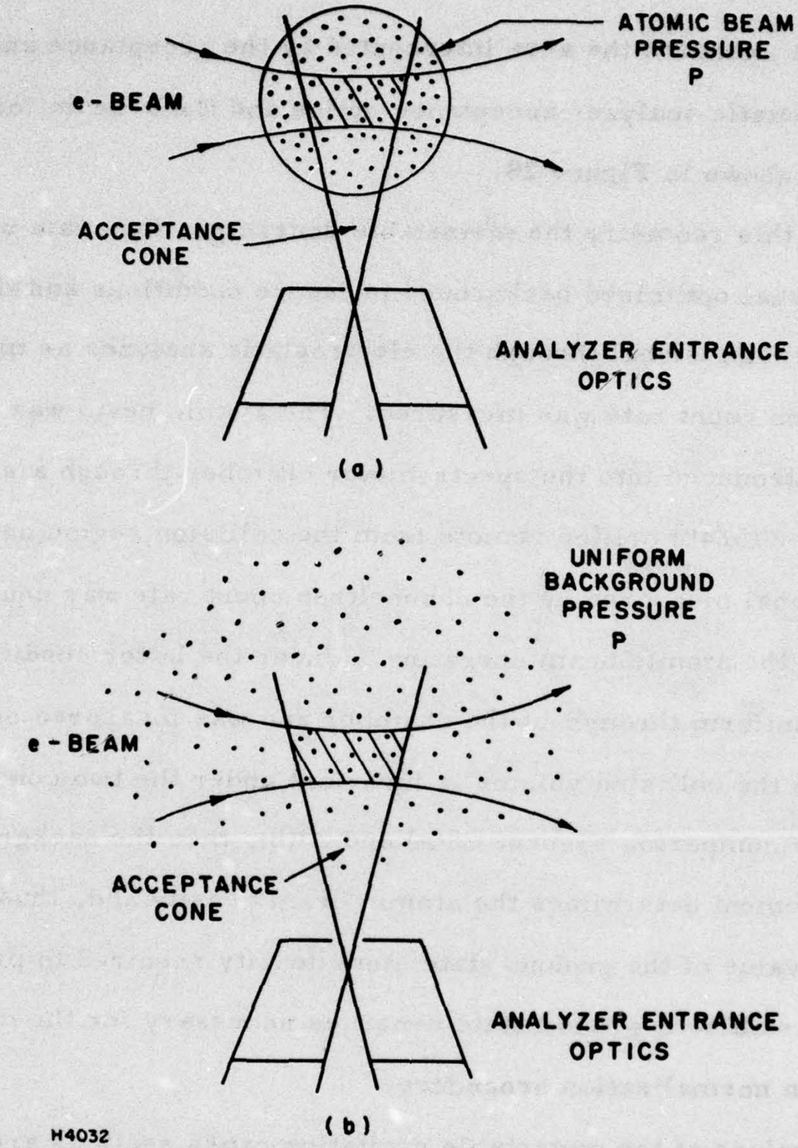

Figure 28 Diagram of the Collision Chamber Geometry Employed for Determining the Atomic Beam Density for the Fluorescence Measurements

(a) Atomic Beam Scattering Measurement

(b) Background Gas Scattering Measurement Note the Identical Interaction Volumes Defined by the Analyzer Entrance Optics

b. Energy Scale Calibration

The $3^3S \rightarrow 2^3P$ transition in helium which was used for normalization of the cross sections was also employed to provide a calibration for the electron energy scale. This transition which has a resonance at threshold as shown in Figure 26, exhibits a vertical onset at 22.72 eV and was used to calibrate the energy scale to an accuracy determined by the e-beam energy distribution which was approximately 0.4 eV.

PRECEDING PAGE NOT FILMED BLANK

III. THEORY

A. INTRODUCTION

There has been considerable recent interest in rare-gas monohalide lasers, due to their potential for high power, high efficiency performance. This has led to an increased understanding of the physics of rare-gas/halogen discharges. In particular, a detailed study[22] of the KrF laser discharge has shown that electron impact excitation of the rare-gas metastables strongly affects the electron energy distribution function and the efficiency of producing the KrF^* upper laser state. The relevant processes are

$$e + Ar^*(3p^5 4s) \rightarrow e + Ar^*(3p^5 n\ell)$$

$$e + Kr^*(4p^5 5s) \rightarrow e + Kr^*(4p^5 n\ell)$$

where $n\ell$ represents higher-lying states. The $p^5 s$ state is split into four levels: $J = 0, 2$ which are truly metastable, and two levels with $J = 1$, which can radiatively decay to the ground state. Under typical laser operating conditions,[22] however, the $J = 1$ states are radiatively-trapped and therefore long-lived. Consequently, all four levels are effectively metastable for the conditions of interest. Calculations have been carried out for the above processes and results for the various cross sections are given in the present report.

B. BASIC FORMULAS

The first Born approximation[23] has been used for the present calculations [although an approximate treatment of strong coupling effects has

(22) Jacob, J.H., and Mangano, J.A., Appl. Phys. Letters 28, 724 (1976).

(23) Moiseiwitsch, B.L., and Smith, S.J., Rev. Mod. Phys. 40, 238 (1968).

been includeu for the dominant s-p transitions (see Section II.D)]. The Born cross section, in units of πa_o^2, for a transition from initial state i to final state f is given by

$$Q_{if} = \frac{8}{k_i^2 \Delta E} \int_{K_{min}}^{K_{max}} f_{if}(K)\, d(\ell n\, K) \tag{1}$$

where k_i^2 is the incident electron energy, $\Delta E = E_f - E_i$ is the transition energy, and $K = \left| \vec{k}_i - \vec{k}_f \right|$ is the magnitude of the momentum change of the incident electron. The quantity $f_{if}(K)$ is the generalized oscillator strength[23] (GOS), and is given by

$$f_{if}(K) = \frac{\Delta E}{K^2} \left| \langle \Psi_f \right| \sum_{j=1}^{N} \exp(i\vec{K} \cdot \vec{r}_j) \left| \Psi_i \rangle \right|^2 \tag{2}$$

where Ψ_i and Ψ_f are the initial and final wavefunctions,of the N-electron atom, respectively.

We start from a single configuration intermediate coupling (IC) wave-function[24] for the rare-gas excited states. Expanding the IC-state in terms of pure LS-coupled basis states, we obtain

$$\left| p^5\, n\ell \Gamma J M \right\rangle = \sum_{SL} \left| p^5\, (^2P) n\ell S L J M \right\rangle \langle S L J | \Gamma J \rangle \tag{3}$$

In the absence of external fields J (the total angular momentum) is a rigorous quantum number in any representation. The expansion coefficients $\langle SLJ | \Gamma J \rangle$ are elements of a unitary matrix, and in general are obtained by diagonalizing the spin-orbit Hamiltonian in the LS-basis states.[24] Transformation matrices between various pure coupling schemes are given in Ref. 25.

(24) Condon, E. U., and Shortley, G. H., The Theory of Atomic Spectra, Cambridge Univ. Press, Cambridge, England (1964).

(25) Cowan, R. D., and Andrew, K. L., J. Opt. Soc. Amer. 55, 502 (1965).

To evaluate the matrix element in formula (2) we use the well-known expansion of the plane wave in spherical harmonics:

$$\exp(i\vec{K}\cdot\vec{r}) = 4\pi \sum_{\lambda\mu} i^{\lambda} j_{\lambda}(Kr)\, Y_{\lambda\mu}^{*}(\widehat{K})\, Y_{\lambda\mu}(\widehat{r}) \tag{4}$$

with $j_\lambda(Kr)$ the spherical Bessel function. Substituting expressions (3) and (4) into (2), summing over final degenerate states and averaging over initial degenerate states, we obtain

$$f_{\Gamma_i J_i,\, \Gamma_f J_f}(K) = \frac{\Delta E}{K^2}\,\frac{4\pi}{2J_i+1} \sum_{\lambda} \Bigg| \sum_{S_i L_i} \sum_{S_f L_f} \langle \Gamma_f J_f \,|\, S_f L_f J_f \rangle$$

$$\times \langle p^5\,({}^2P)\, n_f \ell_f S_f L_f J_f \,\|\, j_\lambda(Kr)\, Y_\lambda(\widehat{r}) \,\|\, p^5\,({}^2P)\, n_i \ell_i S_i L_i J_i \rangle$$

$$\times \langle S_i L_i J_i \,|\, \Gamma_i J_i \rangle \Bigg|^2 \tag{5}$$

The reduced matrix element is evaluated by two applications of Eq. (7.1.8) of Edmonds[26] to give

$$\langle p^5({}^2P) n_f \ell_f S_f L_f J_f \,\|\, j_\lambda(Kr)\, Y_\lambda(\widehat{r}) \,\|\, p^5({}^2P) n_i \ell_i S_i L_i J_i \rangle$$

$$= (-1)^{J_f+S_i+L_i+L_f+\ell_i+\ell_f+1}\, \delta_{S_i,S_f} \sqrt{\frac{(2J_i+1)(2J_f+1)(2L_i+1)(2L_f+1)(2\ell_i+1)(2\ell_f+1)(2\lambda+1)}{4\pi}}$$

$$\times \begin{Bmatrix} L_f & J_f & S_i \\ J_i & L_i & \lambda \end{Bmatrix} \begin{Bmatrix} \ell_f & L_f & 1 \\ L_i & \ell_i & \lambda \end{Bmatrix} \begin{pmatrix} \ell_f & \lambda & \ell_i \\ 0 & 0 & 0 \end{pmatrix} R_\lambda(K) \tag{6}$$

(26) Edmonds, A. R., Angular Momentum in Quantum Mechanics, Princeton Univ. Press, Princeton, New Jersey (1960).

with

$$R_\lambda (K) = \int_0^\infty P_{n_f \ell_f} (r)\, j_\lambda (Kr)\, P_{n_i \ell_i} (r)\, dr \tag{7}$$

and where $P_{n\ell}(r)$ is the radial part of the wavefunction. We have assumed that the various levels of a given configuration can be described by a single radial wavefunction.

For $n_i s$ - $n_f p$ transitions, only the $\lambda = 1$ term provides a non-vanishing contribution, and for this case it is straightforward to show from Eqs. (5) - (7) that

$$f^{(\lambda = 1)}_{\Gamma_i J_i,\, \Gamma_f J_f} (K) = \frac{\Delta E}{K^2} \; \frac{3}{2J_i + 1} \left[\frac{R_1 (K)}{d} \right]^2 \mathcal{S} (\Gamma_f J_f, \Gamma_i J_i) \tag{8}$$

with

$$d = \int_0^\infty P_{n_f p} (r)\, r\, P_{n_i s} (r)\, dr \tag{9}$$

and with $\mathcal{S}$ the optical line strength.[24] Equation (8) can be used to circumvent the spin-orbit diagonalization procedure for cases where either experimental data or intermediate coupling calculations exist for the line strength.

Finally, for various applications it is useful to consider an average excitation cross section between two configurations, which we define as the sum over final $\Gamma_f J_f$-states and the average over initial $\Gamma_i J_i$-states. The average GOS is then given by

$$\bar{f}_{n_i \ell_i,\, n_f \ell_f} (K) = \frac{1}{12\, (2\ell_i + 1)} \sum_{\Gamma_i J_i} \sum_{\Gamma_f J_f} (2J_i + 1)\, f_{\Gamma_i J_i,\, \Gamma_f J_f} (K) \tag{10}$$

Using Eq. (5), together with the unitary property of the expansion matrix and the orthonormality relations for the 6-J symbols,[25] we obtain

$$\bar{f}_{n_i \ell_i, n_f \ell_f}(K) = \frac{\overline{\Delta E}}{K^2}(2\ell_f + 1) \sum_{\lambda} (2\lambda + 1) \begin{pmatrix} \ell_f & \lambda & \ell_i \\ 0 & 0 & 0 \end{pmatrix}^2 \left| R_\lambda (K) \right|^2 \qquad (11)$$

where $\overline{\Delta E}$ is the average transition energy (see Sec. III. C). This is a 1-electron formula, independent of coupling, as expected.

C. RADIAL WAVEFUNCTIONS

The radial wavefunctions are determined from a semi-empirical method,[27] in which the radial Schrodinger equation for the active electron is written in the form

$$\left[\frac{d^2}{dr^2} - \frac{\ell(\ell+1)}{r^2} + \frac{2}{r}\,\zeta\left(\frac{r}{a_{n\ell}}\right) + \tilde{E}_{n\ell}\right] P_{n\ell}(r) = 0 \qquad (12)$$

$\tilde{E}_{n\ell}$ is taken to be the statistically-averaged experimental binding energy of the configuration, $\zeta(\rho)$ is the "effective charge" of the atomic core,[27] and $a_{n\ell}$ is a radial scaling or distortion parameter and is the eigenvalue of Eq. (12) subject to the boundary conditions $P_{n\ell}(0) = P_{n\ell}(\infty) = 0$. The function $\zeta(\rho)$ is given by

$$\zeta(\rho) = (Z - N) + \sum_{j=1}^{N} \int_{\rho}^{\infty} \left(1 - \frac{\rho}{\rho'}\right) P_j^2(\rho')\, d\rho' \qquad (13)$$

with Z the nuclear charge, N the number of core electrons, and $P_j(\rho)$ the radial wavefunctions of the core electrons. For the present calculations, the undistorted core wavefunctions were taken to be the analytical Hartree-Fock functions[28] of the relaxed ion. In the excited state, the active electron

(27) Vainshtein, L. A., Opt. Spect. 3, 313 (1957).

(28) Clementi, E., and Roetti, C., Atomic Data and Nuclear Data Tables 14, 177 (1974).

is fairly far-removed from the core and sees primarily a Coulomb field. The above method should thus give a good representation for the wavefunction in the relevant region of configuration space.

The average experimental binding energies were calculated from the formula

$$\tilde{E}_{n\ell} = \tilde{I} - \left[\sum_J (2J+1)\, E_{n\ell,\, J} \Big/ \sum_J (2J+1) \right] \tag{14}$$

with $\tilde{I}$ the average ionization energy and $E_{n\ell,\, J}$ the excitation energy of each level; all experimental energies for Ar^* and Kr^* were taken from the NBS tables.[29] The values for $\tilde{E}_{n\ell}$, in units of Rydbergs are given in Table I for the states included in the calculation. The average transition energy ($\overline{\Delta E}$) between two configurations is simply the difference between the values listed in the table. The scaling parameters, obtained from the numerical solution of Eq. (12), are given in the last column of Table I. The fact that all of the values of $\alpha_{n\ell}$ are close to unity and that the total variation is only $1.18 \lesssim \alpha_{n\ell} \lesssim 1.27$ provides additional support for the use of the distorted core approximation for the rare-gas excited states.

D. RESULTS AND DISCUSSION

For metastable argon and krypton, transitions of the type $p^5 n_i s$ - $p^5 n_f p$, with $n_f = n_i$, are by far the most important (see below), and both experimental and accurate IC theoretical results for the optical line strengths

(29) Moore, C.E., Atomic Energy Levels, Vols. I and II, Circular of the National Bureau of Standards 467, U.S. Dept. of Commerce, Washington, D.C. (1949).

TABLE I

BINDING ENERGIES AND SCALING PARAMETERS FOR Ar AND Kr

Atom	State	Average Binding Energy, $\lvert E_{n\ell} \rvert$ (Rydbergs)	Scaling Parameter, $\alpha_{n\ell}$
Ar	$3p^5 4s$	0.30627	1.2718
	4p	0.19464	1.2343
	3d	0.12740	1.2490
	5s	0.12376	1.2512
	5p	0.09183	1.2204
	4d	0.07174	1.2383
Kr	$4p^5 5s$	0.29700	1.2245
	5p	0.18593	1.1915
	4d	0.13321	1.2228
	6s	0.12006	1.2012
	6p	0.08867	1.1796
	5d	0.07312	1.2104

exist in the literature for these cases.[30-33] Equation (8) has therefore been used to obtain a large number of Born cross sections for the Ar^* (4s - 4p) and Kr^* (5s - 5p) transition arrays.[34] The effect of choosing different coupling schemes to represent the excited states is shown in Figures 29 and 30. Referring to the Ar^* (4s - 4p) array, Figure 29 shows the Born cross section vs incident electron energy for the $1s_2 - 2p_4$ transition (see Ref. 29 for notation) obtained with the experimental line strength;[30] and with line strengths calculated in intermediate, LS-, and $j\ell$-coupling;[31] Figure 30 shows the corresponding results for the $1s_5 - 2p_8$ transition. In both cases, the IC results are very close to those obtained using the experimental $\mathcal{S}$ values. In the $1s_2 - 2p_4$ case, the pure $j\ell$-coupling cross section is in reasonably good agreement with the IC curve, while the LS-coupling cross section is in very poor agreement. For the $1s_5 - 2p_8$ transition, however, just the opposite is true. Furthermore, again with respect to the Ar^* (4s - 4p) array, the $1s_2 - 2p_6$ transition is completely forbidden in both $j\ell$- and LS-coupling,[31] while the IC calculation gives a large cross section with a peak value of $36\,\pi a_o^2$. The cross section clearly can be very sensitive to the choice of coupling scheme, and intermediate coupling should be used to obtain reliable results.

(30) Wiese, W. L., Smith, M. W., and Miles, B. M., Atomic Transition Probabilities, Vol. II, NSRDS-NBS 22, U.S. Dept. of Commerce, Washington, D.C. (1969).

(31) Garstang, R.H., and VanBlerkom, J., J. Opt. Soc. Amer. 55, 1054 (1965).

(32) Murphy, P.W., J. Opt. Soc. Amer. 58, 1200 (1968).

(33) The authors of Refs. 31-32 give transition probabilities or Einstein A-factors in intermediate coupling. The corresponding line strength, in atomic units, is obtained from the relation $\mathcal{S} = 4.95 \times 10^{-19}\, g_u \lambda^3 A$, with g_u the statistical weight of the upper level, λ the transition wavelength in Å, and A the transition probability in sec^{-1}.

(34) Hyman, H. A., (unpublished).

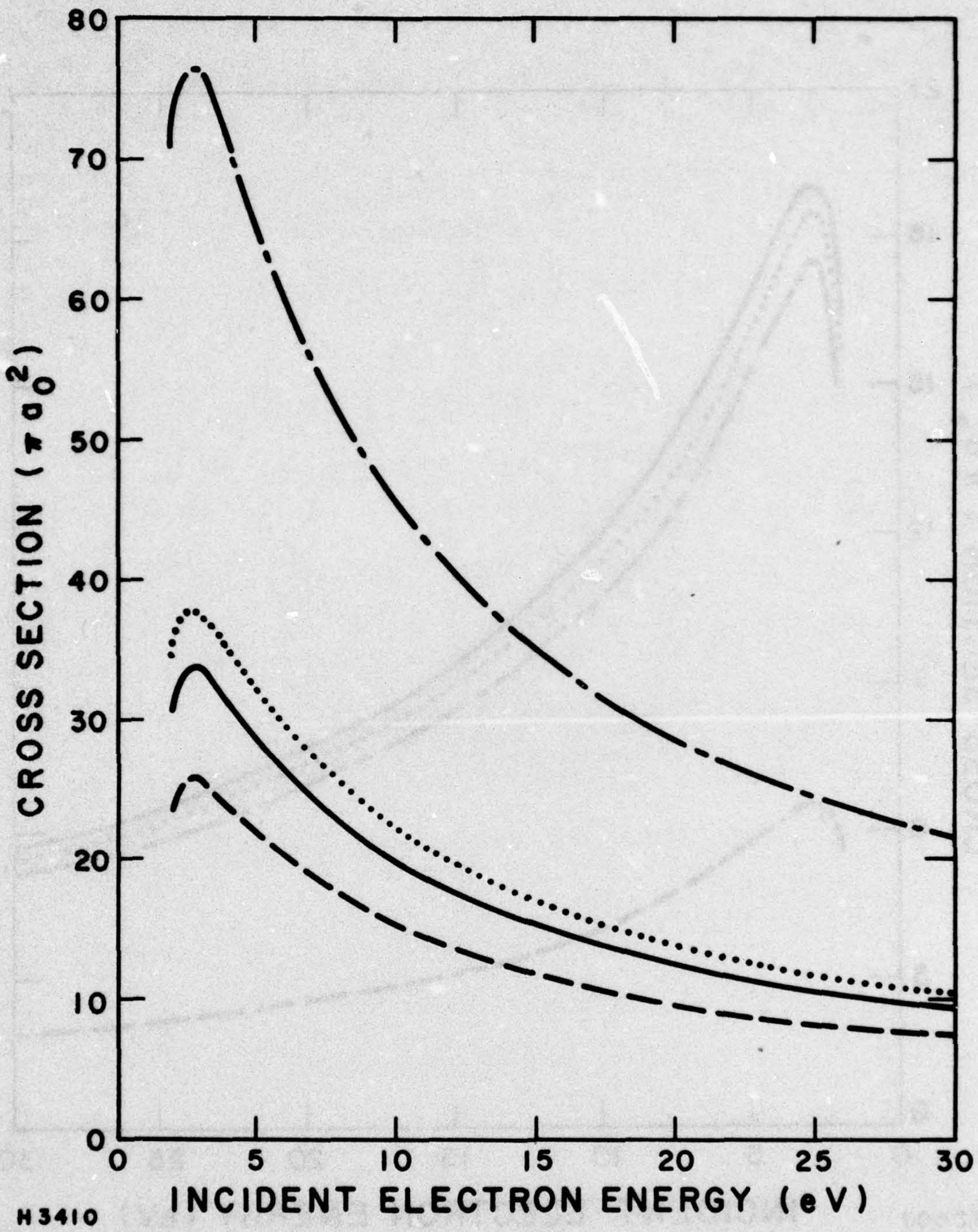

Figure 29 Born Cross Section vs Incident Electron Energy for the $1s_2$ - $2p_4$ Transition of Ar^*: (———) Intermediate Coupling, (— — — —) $j\ell$ -Coupling, (—— - ——) LS-Coupling, (. . . . .) Experimental Line Strength

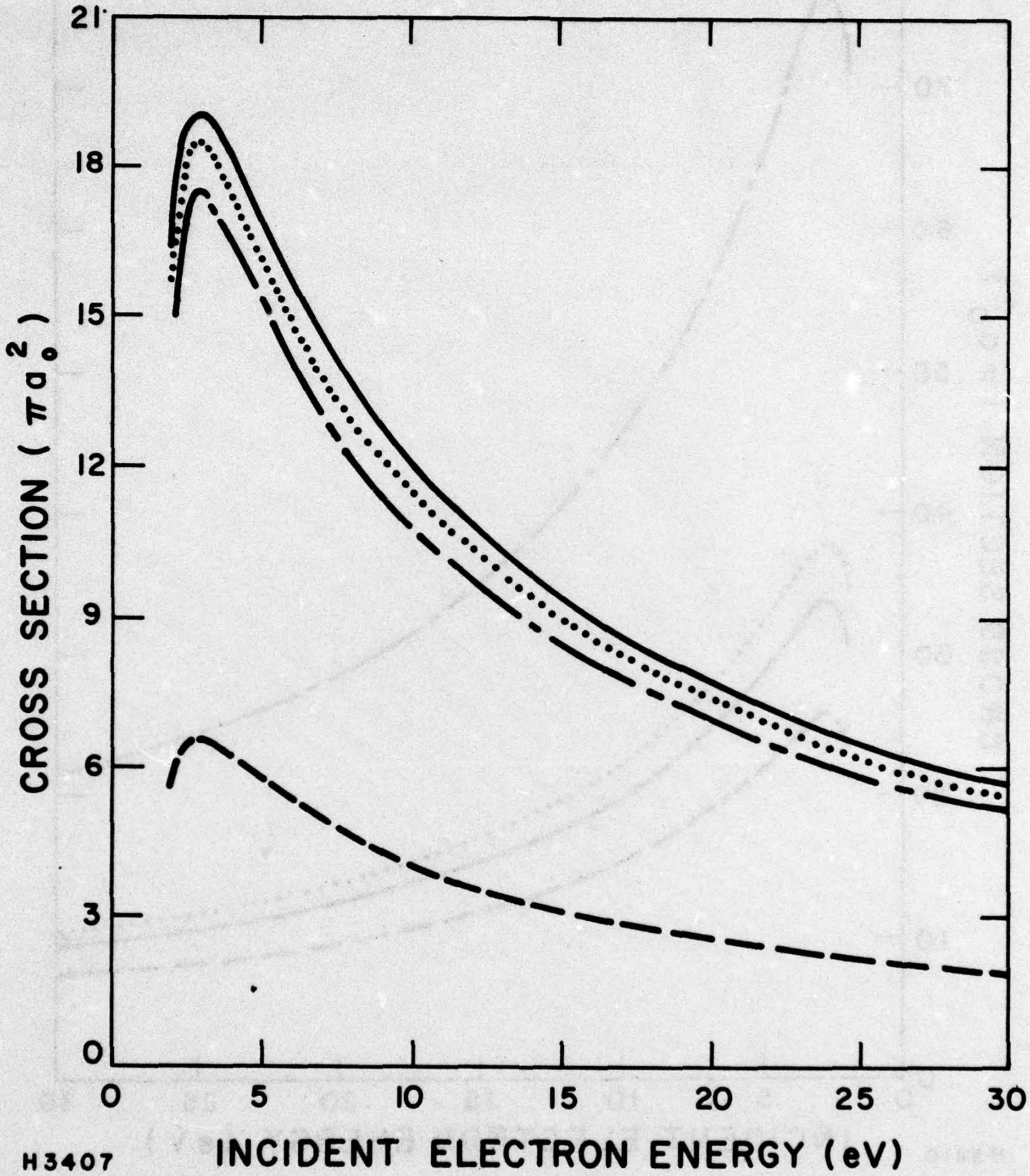

Figure 30 Born Cross Section vs Incident Electron Energy for the $1s_5$ - $2p_8$ Transition of Ar*: (———) Intermediate Coupling, (— — — —) jℓ-Coupling, (——— – ———) LS-Coupling (. . . . .) Experimental Line Strength

The average Born cross sections, calculated from Eq. (11), are shown as the solid curves in Figures 31 and 32, for the cases Ar^* (4s - nℓ) and Kr^* (5s - nℓ). As indicated earlier, the s-p transition with no change in principal quantum number is the dominant process. This is due to the long-range dipole interaction, which causes the s and p states to be strongly coupled and which in turn causes a breakdown in the Born approximation in the low to intermediate energy range. Seaton has introduced a simplified impact parameter theory,[35] which accounts approximately for both the weak coupling and strong coupling regimes. The method requires a knowledge of the oscillator strength, f and of the cut-off radius,[35] R_o. The average oscillator strength was determined from Eq. (11), together with the wellknown relation

$$\bar{f}_{n_i s,\, n_f p} = \lim_{K \to 0} \bar{\mathcal{f}}_{n_i s,\, n_f p}(K) \tag{15}$$

while the cut-off radius was chosen so as to give agreement with the Born theory at high energies. The parameters used in the calculations were: for Ar^* (4s - 4p), $\bar{f} = 1.068$ and $R_o = 4.572\,a_o$; for Kr^* (5s - 5p), $\bar{f} = 1.121$ and $R_o = 4.723\,a_o$. The results of the impact parameter theory are given by the dashed curve in Figures 31 and 32. Strong coupling effects are dominant at incident energies $E_i \lesssim 20$ eV, and the resulting cross sections are seen to differ significantly from the Born theory both in shape as well as in magnitude.

Finally, we consider the average optical excitation cross section,[36,37] $\overline{Q}_T$, for the Ar^* (4s - 4p) and Kr^* (5s - 5p) transitions. This quantity, defined

---

(35) Seaton, M.J., Proc. Phys. Soc. 79, 1105 (1962).

(36) Chen, S.T., and Gallagher, A.C., Phys. Rev. A14, 593 (1976).

(37) Chen, S.T., and Gallagher, A.C., Phys. Rev. A (to be published).

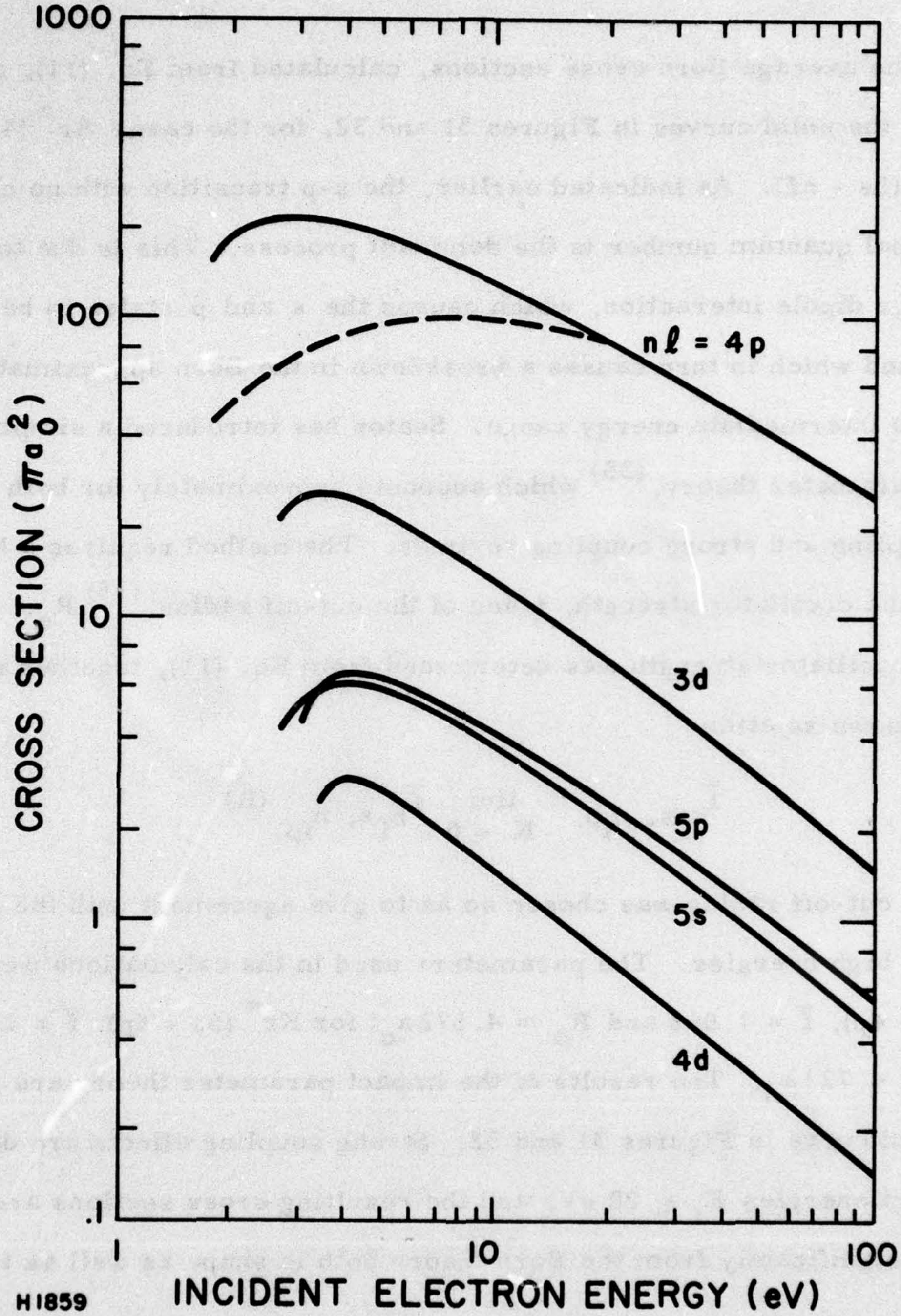

Figure 31 **Average Cross Sections vs Incident Energy for the Configurations Ar* ($3p^5$ 4s - $3p^5$ nℓ): (———) Born Theory, (— — —) Impact Parameter Theory**

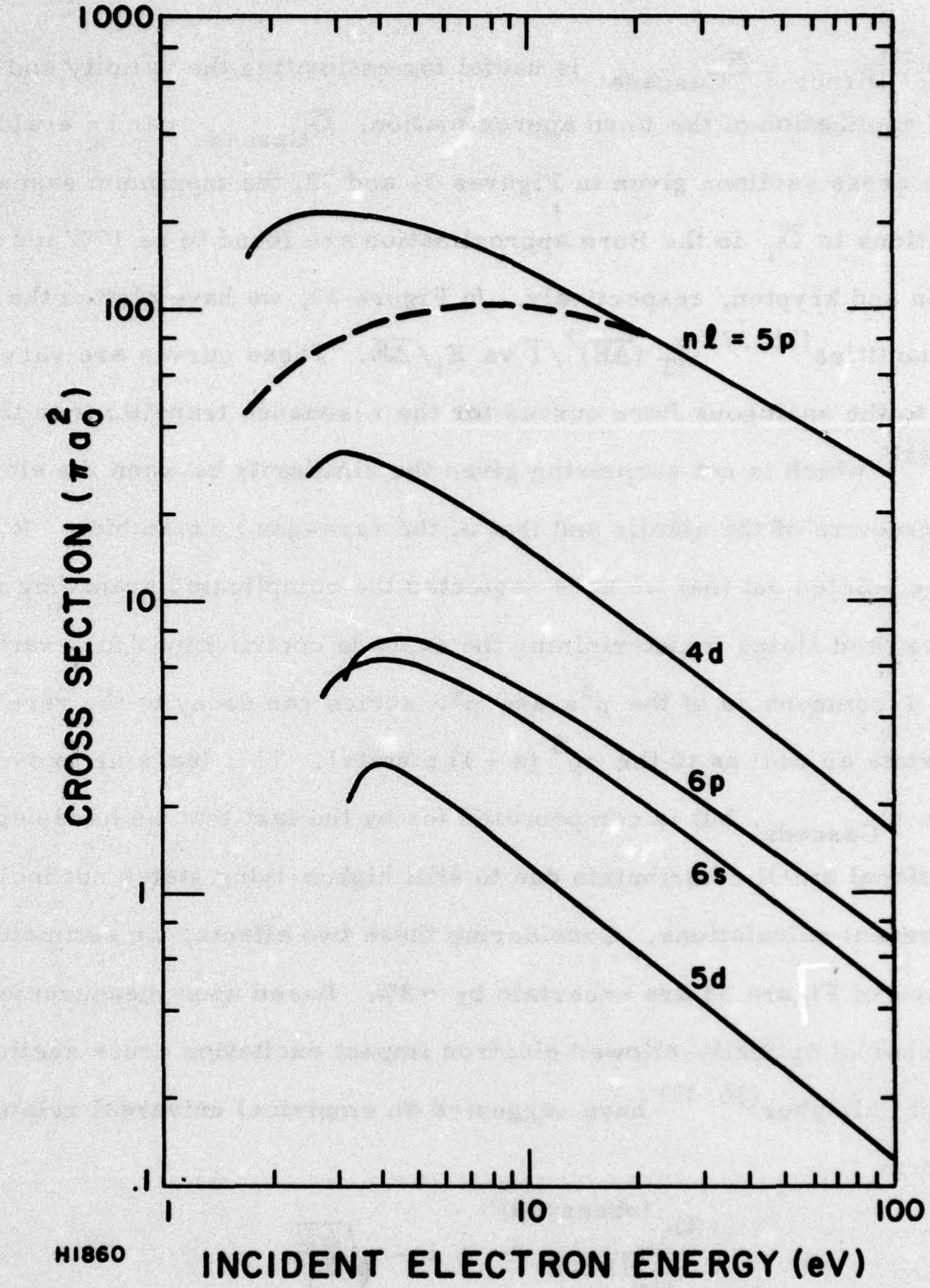

Figure 32 **Average Cross Section vs Incident Electron Energy for the Configurations Kr* ($4p^5\ 5s$ - $4p^5\ n\ell$): (————) Born Theory (— — —) Impact Parameter Theory**

by $\overline{Q}_T = \overline{Q}_{Direct} + \overline{Q}_{Cascade}$, is useful for estimating the validity and range of application of the Born approximation. $\overline{Q}_{Cascade}$ can be evaluated from the cross sections given in Figures 31 and 32; the maximum cascade contributions to $\overline{Q}_T$ in the Born approximation are found to be 17% and 18% for argon and krypton, respectively. In Figure 33, we have plotted the reduced quantities[36, 37] $\overline{Q}_T\ (\overline{\Delta E})^2/\overline{f}$ vs $E_i/\overline{\Delta E}$. These curves are very similar to the analogous Born curves for the resonance transitions in the alkalis,[37] which is not surprising given the similarity between the electronic structure of the alkalis and that of the rare-gas metastables. It should be pointed out that we have neglected the complicated branching ratios for the excited states in determining the cascade contribution [for example, the J = 1 components of the p^5s and p^5d series can decay to the rare-gas ground state as well as to the $np^5\ (n+1)\ p$ state]. This leads us to overestimate $\overline{Q}_{Cascade}$, but is compensated for by the fact that we have neglected the additional small contribution due to still higher-lying states not included in the present calculations. Considering these two effects, we estimate that the curves of Figure 33 are uncertain by ~3%. Based upon measurements of a number of optically-allowed electron impact excitation cross sections, Chen and Gallagher[36, 37] have suggested an empirical universal relation of the form.

$$\frac{Q_T^{(observed)}}{Q_T^{(Born)}} \approx 1 - \sqrt{\frac{\Delta E}{E_i}} \tag{16}$$

which would imply that the Born theory is no worse than a factor of 2 in error for incident energies as low as $E_i \sim 6$ eV for the present case. Furthermore, Seaton's method[35] appears capable of removing ~ 3/4 of the discrepancy between the observed and Born cross sections in this energy range.

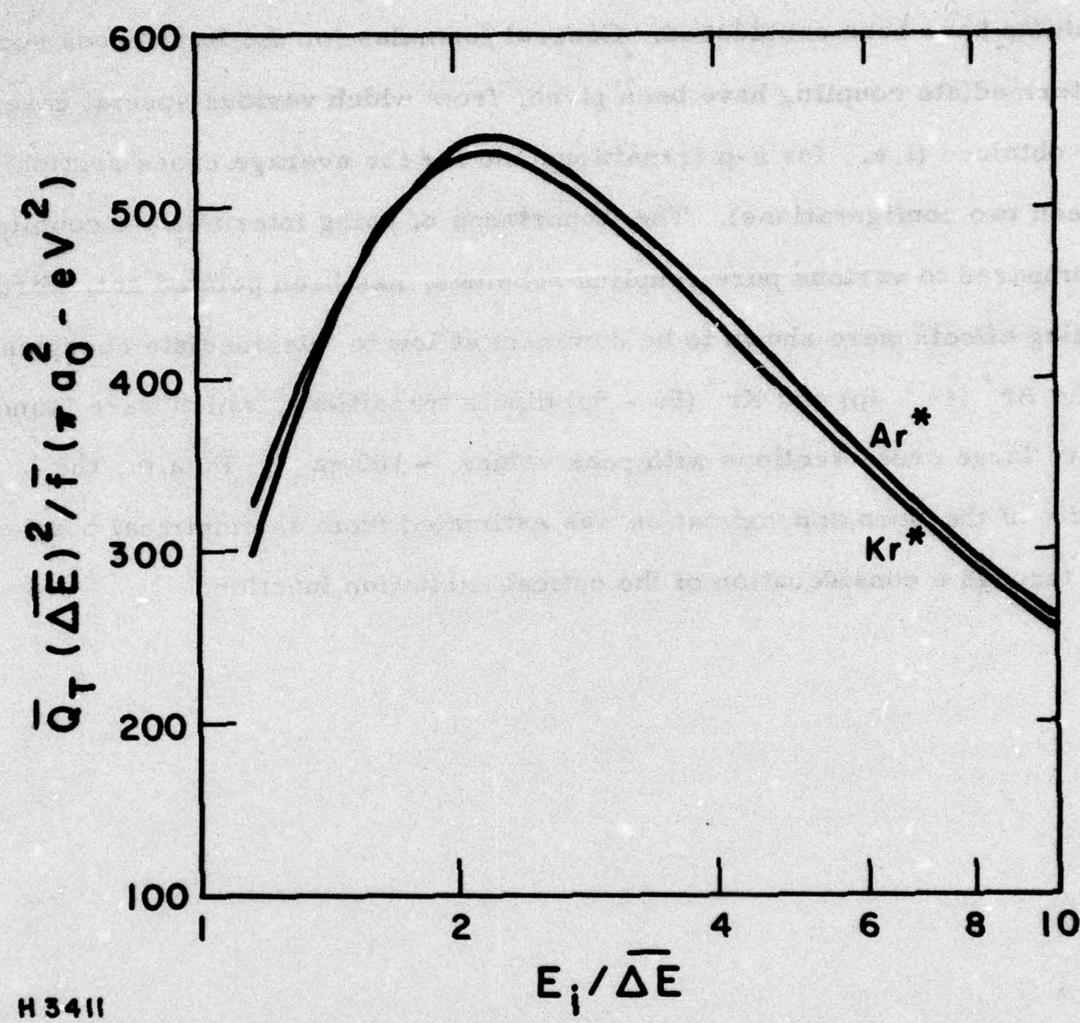

Figure 33 $\bar{Q}_T (\overline{\Delta E})^2/\bar{f}$ vs $E_i/\overline{\Delta E}$ for the Transitions Ar* (4s - 4p) and Kr* (5s - 5p). $\bar{Q}_T$ is the average Born cross section including cascades, $\overline{\Delta E}$ is the transition energy, $\bar{f}$ is the oscillator strength, and E_i is the incident electron energy

E. CONCLUSION

Electron impact excitation processes for metastable argon and krypton atoms have been considered. General formulas for the Born cross section in intermediate coupling have been given, from which various special cases were obtained (i.e., for s-p transitions and for the average cross section between two configurations). The importance of using intermediate coupling, as compared to various pure coupling schemes, has been pointed out. Strong coupling effects were shown to be dominant at low to intermediate energies for the Ar^* (4s - 4p) and Kr^* (5s - 5p) dipole transitions, which were found to have large cross sections with peak values $\sim 100\ \pi a_o^2$. Finally, the validity of the Born approximation was estimated from an empirical point of view through a consideration of the optical excitation function.

REFERENCES

1. "KrF Laser Research," AERL 804, April 1976.
2. Long, D.R., and Geballe, R., Phys. Rev. 1, 260 (1970).
3. Lake, M. L. and Garscadden, A., 28th Gaseous Electronics Conference, Rolla, Mo. (1975), Paper C-5.
4. Mityurwa, A.A., and Penkin, N.P., Opt. Spectrosc. 38, 229 (1975).
5. Wilson, W.G., and Williams, W.L., J. Phys. B9, 423 (1976).
6. Tanne, P.D., "Cumulative Ionization and Excitation of Molecular Nitrogen Metastables by Electron Impact," Dissertation (1973), School of Engineering, Air Force Institute of Technology.
7. Ewing, J.J., and Brau, C.A., Appl. Phys. Lett. 27, 350 (1975).
8. Ewing, J.J., and Brau, C.A., Phys. Rev. A12, 129 (1975).
9. Mangano, J.A., and Jacob, J.H., Appl. Phys. Lett. 27, 495 (1975).
10. Burke, P.G., Cooper, J.W., Ormande, S., and Taylor, A.J., Abstract V ICPEAC, Liningrad, (1967).
11. "Investigation of Electron Impact Processes Relevant to Visible Lasers." Boness, M.J., and Hyman, H.A., AERL Semi-Annual Report, March 1977-Aug. 1977.
12. Peterson, J.R., and Lorentz, D.C., Phys. Rev. 182, 152 (1969).
13. Neynaber, R.H., and Magnuson, G.D., J. Chem. Phys. 65, 5239 (1976).
14. Stebbings, R.F., Proc. Roy. Soc. 241, 270 (1957).
15. "Investigation of Electron Impact Processes Relevant to Visible Laser." Boness, M.J., and Hyman, H.A., AERL Semi-Annual Report, Sept 1975-Feb. 1976.
16. "Investigation of Electron Impact Processes Relevant to Visible Lasers." Boness, M.J., and Hyman, H.A., AERL Semi-Annual Report, March 1976-Aug. 1976.
17. "Investigation of Electron Impact Processes Relevant to Visible Lasers." Boness, M.J., and Hyman, H.A., AERL Semi-Annual Report, Sept. 1976-Feb. 1977.

18. Jobe, J.D. & St. John, R.H., Phys. Rev. 164, 117-121 (1967).

19. Zapesochnyi, I.P., and Feltsan, P.V., Optika i Spektrosak (USSR), 20, 521 (1966) English translation in: Optics & Spectrosc (U.S.A.) 20, 291 (1966).

20. Lilly, R.A., J. Opt. Soc. Am. 66, 245 (1976).

21. Dunning, F.B., Rundel, R.D., and Slebbings, R.F., Rev. Sci. Inst. 46, 697 (1975).

22. Jacob, J.H., and Mangano, J.A., Appl. Phys. Letters 28, 724 (1976).

23. Moiseiwitsch, B.L., and Smith, S.J., Rev. Mod. Phys. 40, 238 (1968).

24. Condon, E.U., and Shortley, G.H., The Theory of Atomic Spectra, Cambridge Univ. Press, Cambridge, England (1964).

25. Cowan, R.D., and Andrew, K.L., J. Opt. Soc. Amer. 55, 502 (1965).

26. Edmonds, A.R., Angular Momentum in Quantum Mechanics, Princeton Univ. Press, Princeton, New Jersey (1960).

27. Vainshtein, L.A., Opt. Spect. 3, 313 (1957).

28. Clementi, E., and Roetti, C., Atomic Data and Nuclear Data Tables 14, 177 (1974).

29. Moore, C.E., Atomic Energy Levels, Vols. I and II, Circular of the National Bureau of Standards 467, U.S. Dept. of Commerce, Washington, D.C. (1949).

30. Wiese, W.L., Smith, M.W., and Miles, B.M., Atomic Transition Probabilities, Vol. II, NSRDS-NBS 22, U.S. Dept. of Commerce, Washington D.C. (1969).

31. Garstang, R.H., and VanBlerkom, J., J. Opt. Soc. Amer. 55, 1054 (1965).

32. Murphy, P.W., J. Opt. Soc. Amer. 58, 1200 (1968).

33. The authors of Refs. 31-32 give transition probabilities or Einstein A-factors in intermediate coupling. The corresponding line strength, in atomic units, is obtained from the relation $\mathcal{L} = 4.95 \times 10^{-19} g_u \lambda^3 A$, with g_u the statistical weight of the upper level, λ the transition wavelength in Å, and A the transition probability in sec^{-1}.

34. Hyman, H.A., (unpublished).

35. Seaton, M.J., Proc. Phys. Soc. 79, 1105 (1962).

36. Chen, S.T., and Gallagher, A.C., Phys. Rev. A14, 593 (1976).

37. Chen, S.T., and Gallagher, A.C., Phys. Rev. A (to be published).

DISTRIBUTION LIST

Office of Naval Research, Department of the Navy, Arlington, VA 22217 - Attn: Physics Program (3 copies)
Naval Research Laboratory, Department of the Navy, Washington, D.C. 20375 - Attn: Technical Library (1 copy)
Office of the Director of Defense, Research and Engineering, Information Office Library Branch, The Pentagon, Washington, D.C. 20301 (1 copy)
U.S. Army Research Office, Box CM, Duke Station, Durham, N.C. 27706 (1 copy)
Defense Documentation Center, Cameron Station, Alexandria, VA 22314 (12 copies)
Defender Information Analysis Center, Battelle Memorial Institute, 505 King Avenue, Columbus, OH 43201 (1 copy)
Commanding Officer, Office of Naval Research Branch Office, 536 South Clark Street, Chicago, IL 60615 (1 copy)
New York Area Office, Office of Naval Research, 715 Broadway (5th Floor), New York, NY 10003 - Attn: Dr. Irving Rowe
San Francisco Area Office, Office of Naval Research, 760 Market Street, Room 447, San Francisco, CA 94102 (1 copy)
Air Force Office of Scientific Research, Department of the Air Force, Washington, D.C. 22209 (1 copy)
Office of Naval Research Branch Office, 1030 East Green Street, Pasadena, CA 91106 - Attn: Dr. Robert Behringer (1 copy)
Code 102 IP (ONRL), Office of Naval Research, 800 N. Quincy Street, Arlington, VA 22217 (1 copy)
Defense Advanced Research Projects Agency, 1400 Wilson Blvd., Arlington, VA 22209 - Attn: Strategic Technology Office (1 copy)
Office Director of Defense, Research and Engineering, The Pentagon, Washington, D.C. 20301 - Attn: Assistant Director (Space and Advanced Systems) (1 copy)
Office of the Assistant Secretary of Defense, System Analysis (Strategic Programs), Washington, D.C. 20301 - Attn: Mr. Gerald R. McNichols (1 copy)
U.S. Arms Control and Disarmament Agency, Dept. of State Bldg., Rm. 4931, Washington, D.C. 20451 - Attn: Mr. Charles Henkin (1 copy)
Energy Research Development Agency, Division of Military Applications, Washington, D.C. 20545 (1 copy)
National Aeronautics and Space Administration, Lewis Research Center, Cleveland, OH 44135 - Attn: Dr. John W. Dunning, Jr. (1 copy)
(Aerospace Research Engineer)
National Aeronautics and Space Administration, Code RR, FOB 10B, 600 Independence Ave., SW, Washington, D.C. 20546 (1 copy)
National Aeronautics and Space Administration, Ames Research Center, Moffett Field, CA 94035 - Attn: Dr. Kenneth W. Billman (1 copy)
Department of the Army, Office of the Chief of RD&A, Washington, D.C. 20310 - Attn: DARD-DD (1 copy)
DAMA-WSM-T (1 copy)
Department of the Army, Office of the Deputy Chief of Staff for Operations and Plans, Washington, D.C. 20310 - Attn: DAMO-RQD (1 copy)
U.S. Army Missile Command, Research and Development Division, Redstone Arsenal, AL 35809 - Attn: Army High Energy Laser Programs (2 copies)
Commanding Officer, U.S. Army Mobility Equipment R&D Center, Ft. Belvoir, VA 22060 - Attn: SMEFB-MW (1 copy)
Commander, U.S. Army Armament Command, Rock Island, IL 61201 - Attn: AMSAR-RDT (1 copy)
Director, Ballistic Missile Defense Advanced Technology Center, P.O. Box 1500, Huntsville, AL 35807 - Attn: ATC-O (1 copy)
ATC-T (1 copy)
Commanding General, U.S. Army Munitions Command, Dover, NH 17801 - Attn: Mr. Gilbert F. Chesnov (AMSMU-R) (1 copy)
Director, U.S. Army Ballistics Res. Lab, Aberdeen Proving Ground, MD 21005 - Attn: Dr. Robert Eichenberger (1 copy)
Commandant U.S. Army, Air Defense School, Ft. Bliss, TX 79916 - Attn: Air Defense Agency (1 copy)
ATSA-CTD-MS (1 copy)
Commanding General, U.S. Army Combat Dev. Command, Ft. Belvoir, VA 22060 - Attn: Director of Material, Missile Div. (1 copy)
Commander, U.S. Army Training & Doctrine Command, Ft. Monroe, VA 23651 - Attn: ATCD-CF (1 copy)
Commander, U.S. Army Electronics Command, Ft. Monmouth, NJ 07703 - Attn: AMSEL-CT-L, Dr. R.G. Buser (1 copy)
Commander, U.S. Army Combined Arms Combat Developments Activity, Ft. Leavenworth, KS 66027 (1 copy)
National Security Agency, Ft. Geo. G. Meade, MD 20755 - Attn: R.C. Foss A763 (1 copy)
Deputy Commandant for Combat & Training Developments, U.S. Army Ordnance Center and School, Aberdeen Proving Ground, MD 21005 - Attn: ATSL-CTD-MS-R (1 copy)
Department of the Navy, Office of the Chief of Naval Operations, The Pentagon 5C739, Washington, D.C. 20350 - Attn: (OP 982F3) (1 copy)
Office of Naval Research Branch Office, 495 Summer Street, Boston, MA 02210 - Attn: Dr. Fred Quelle (1 copy)
Department of the Navy, Deputy Chief of Navy Material (Dev.), Washington, D.C. 20360 - Attn: Mr. R. Gaylord (Mat 032B) (1 copy)
Naval Missile Center, Point Mugu, CA 93042 - Attn: Gary Gibbs (Code 5352) (1 copy)
Naval Research Laboratory, Washington, D.C., 20375 - Attn: Electro-Optical Technology, Program Office, Code 1409 (1 copy)
Dr. P. Livingston - Code 5560 (1 copy)
Dr. A.I. Schindler - Code 6000 (1 copy)
Dr. John L. Walsh - Code 5503 (1 copy)
High Energy Laser Project Office, Department of the Navy, Naval Sea System Command, Washington, D.C. 20360 - Attn: Capt. A. Skolnick, USN (PM 22) (1 copy)
Superintendent, Naval Postgraduate School, Monterey, CA 93940 - Attn: Library (Code 2124) (1 copy)
Navy Radiation Technology, Air Force Weapons Lab (NLO), Kirtland AFB, NM 87117 (1 copy)
Naval Surface Weapons Center, White Oak, Silver Spring, MD 20910 - Attn: Dr. Leon H. Schindel (Code 310) (1 copy)
Dr. E. Leroy Harris (Code 313) (1 copy)
Mr. K. Enkenhaus (Code 034) (1 copy)
Mr. J. Wise (Code 047) (1 copy)
Technical Library (1 copy)
U.S. Naval Weapons Center, China Lake, CA 93555 - Attn: Technical Library (1 copy)
HQ USAF (AF/RDPS), The Pentagon, Washington, D.C. 20330 - Attn: Lt. Col. A.J. Chiota (1 copy)
HQ AFSC/XRLW, Andrews AFB, Washington, D.C. 20331 - Attn: Maj. J.M. Walton (1 copy)
HQ AFSC (DLCAW) Andrews AFB, Washington, D.C. 20331 - Attn: Maj. H. Axelrod (1 copy)
Air Force Weapons Laboratory, Kirtland AFB, NM 87117 - Attn: LR (1 copy)
AL (1 copy)
HQ Aeronautical Systems Div., Wright Patterson AFB, OH 45433 - Attn: XRF - Mr. Clifford Fawcett (1 copy)
Rome Air Development Command, Griffiss AFB, Rome, NY 13440 - Attn: Mr. R. Urtz (OCSE) (1 copy)
HQ Electronics Systems Div. (ESL), L.G. Hanscom Field, Bedford, MA 01730 - Attn: Mr. Alfred E. Anderson (XRT) (1 copy)
Technical Library (1 copy)
Air Force Rocket Propulsion Lab, Edwards AFB, CA 93523 - Attn: B.R. Bornhorst, (LKCG) (1 copy)
Air Force Aero Propulsion Lab, Wright Patterson AFB, OH 45433 - Attn: Col. Walter Moe (CC) (1 copy)
Dept. of the Air Force, Foreign Technology Division, Wright Patterson AFB, OH 45433 - Attn: PDTN (1 copy)
Commandant of the Marine Corps, Scientific Advisor (Code RD-1), Washington, D.C. 20380 (1 copy)

DISTRIBUTION LIST (continued)

Aerospace Research Labs, (AP), Wright Patterson AFB, OH 45433 - Attn: Lt. Col. Max Duggins (1 copy)
Defense Intelligence Agency, Washington, D.C. 20301 - Attn: Mr. Seymour Berler (DTIB) (1 copy)
Central Intelligence Agency, Washington, D.C. 20505 - Attn: Mr. Julian C. Nall (1 copy)
Analytic Services, Inc., 5613 Leesburg Pike, Falls Church, VA 22041 - Attn: Dr. John Davis (1 copy)
Aerospace Corp., P. O. Box 92957, Los Angeles, CA 90009 - Attn: Dr. G. P. Milburn (1 copy)
Airesearch Manuf. Co., 9851-9951 Sepulveda Blvd., Los Angeles, CA 90009 - Attn: Mr. A. Colin Stancliffe (1 copy)
Atlantic Research Corp., Shirley Highway At Edsall Road, Alexandria, VA 22314 - Attn: Mr. Robert Naismith (1 copy)
Avco Everett Research Lab., 2385 Revere Beach Parkway, Everett, MA 02149 - Attn: Dr. George Sutton (1 copy)
Dr. Jack Daugherty (1 copy)
Battelle Columbus Laboratories, 505 King Avenue, Columbus, OH 43201 - Attn: Mr. Fred Tietzel (STPIAC) (1 copy)
Bell Aerospace Co., Buffalo, NY 14240 - Attn: Dr. Wayne C. Solomon (1 copy)
Boeing Company, P. O. Box 3999, Seattle, WA 98124 - Attn: Mr. M. I. Gamble (2-, 460, MS 8C-88) (1 copy)
Electro-Optical Systems, 300 N. Halstead, Pasadena, CA 91107 - Attn: Dr. Andrew Jensen (1 copy)
ESL Inc., 495 Java Drive, Sunnyvale, CA 94086 - Attn: Arthur Einhorn (1 copy)
General Electric Co., Space Division, P. O. Box 8555, Philadelphia, PA 19101 - Attn: Dr. R. R. Sigismonti (1 copy)
General Electric Co., 100 Plastics Avenue, Pittsfield, MA 01201 - Attn: Mr. D. G. Harrington (Rm. 1044) (1 copy)
General Research Corp., P. O. Box 3587, Santa Barbara, CA 93105 - Attn: Dr. R. Holbrook (1 copy)
Hercules, Inc., Industrial Dept., Wilmington, DC 19899 - Attn: Dr. R.S. Voris (1 copy)
Hercules, Inc., P. O. Box 210, Cumberland, MD 21502 - Attn: Dr. Ralph R. Preckel (1 copy)
Hughes Research Labs, 3011 Malibu Canyon Road, Malibu, CA 90265 - Attn: Dr. D. Forster (1 copy)
Hughes Aircraft Co., Aerospace Group-Systems Division, Canoga Park, CA 91304 - Attn: Dr. Jack A. Alcalay (1 copy)
Hughes Aircraft Co., Centinela and Tenale Streets, Building 6, MS E-125, Culver City, CA 90230 - Attn: Dr. William Yates (1 copy)
Institute for Defense Analyses, 400 Army-Navy Drive, Arlington, Va. 22202 - Attn: Dr. Alvin Schnitzler (1 copy)
Johns Hopkins University, Applied Physics Lab, 8621 Georgia Avenue, Silver Spring, Md. 20910 - Attn: Dr. Albert M. Stone (1 copy)
Lawrence Livermore Laboratory, P. O. Box 808, Livermore, CA 94550 - Attn: Dr. R. E. Kidder (1 copy)
Dr. E. Teller (1 copy)
Dr. Joe Fleck (1 copy)
Los Alamos Scientific Laboratory, P. O. Box 1663, Los Alamos, NM 87544 - Attn: Dr. Keith Boyer (1 copy)
Lulejian and Associated, Inc., Del Amo Financial Center, 21515 Hawthorne Blvd. - Suite 500, Torrance, CA 90503 (1 copy)
Lockheed Palo Alto Research Lab, 3251 Hanover Street, Palo Alto, CA 94303 - Attn: L. R. Lunsford, ORGN. 52-24, Bldg. 201 (1 copy)
Mathematical Sciences Northwest, Inc., P. O. Box 1887, Bellevue, WN 98009 - Attn: Dr. Abraham Hertzberg (1 copy)
Massachusetts Institute of Technology, Lincoln Laboratory, P. O. Box 73, Lexington, MA 02173 - Attn: Dr. S. Edelberg (1 copy)
Dr. L. C. Marquet (1 copy)
McDonnell Douglas Astronautics Co., 5301 Bolsa Avenue, Huntington Beach, CA 92647 - Attn: Mr. P. L. Klevatt, Dept. A3-830-BBFO, M/S9 (1 copy)
McDonnell Douglas Research Labs, Dept. 220, Box 516, St. Louis, MO 63166 - Attn: Dr. D. P. Ames (1 copy)
North American Rockwell Corp., Autonetics Div., Anaheim, CA 92803 - Attn: Mr. T. T. Kumagi, C/476 Mail Code HA18 (1 copy)
Northrop Corp., 3401 West Broadway, Hawthorne, CA 90250 - Attn: Dr. Gerard Hasserjian, Laser Systems Dept. (1 copy)
Dr. Anthony N. Pirri, 30 Commerce Way, Woburn, MA 01801 (1 copy)
Rand Corp., 1700 Main Street, Santa Monica, CA 90406 - Attn: Dr. C. R. Culp/Mr. G. A. Carter (1 copy)
Raytheon Co., 28 Seyon Street, Waltham, MA 02154 - Attn: Dr. F. A. Horrigan (Res. Div.) (1 copy)
Raytheon Co., Boston Post Road, Sudbury, Ma. 01776 - Attn: Dr. C. Sonnenschien (Equip. Div.) (1 copy)
Raytheon Co., Bedford Labs, Missile Systems Div., Bedford, MA 01730 - Attn: Dr. H. A. Mehlhorn (1 copy)
Riverside Research Institute, 80 West End Street, New York, NY 10023 - Attn: Dr. L. H. O'Neil (1 copy)
Dr. John Bose (1 copy)
(HPEGL Library) (1 copy)
Rockwell International Corporation, Rocketdyne Division, Albuquerque District Office, 3636 Menaul Blvd., NE, Suite 211, Albuquerque, NM 87110,
Attn: C.K. Kraus, Mgr. (1 copy)
Sandia Corp., P.O. Box 5800, Albuquerque, NM 87115 - Attn: Dr. Al Narath (1 copy)
Stanford Research Institute, Menlo Park, CA 94025 - Attn: Dr. F. T. Smith (1 copy)
Science Applications, Inc., 1911 N. Ft. Meyer Drive, Arlington, VA 22209 - Attn: L. Peckham (1 copy)
Science Applications, Inc., P. O. Box 328, Ann Arbor, MI 48103 - Attn: R. E. Meredith (1 copy)
Science Applications, Inc., 6 Preston Court, Bedford, MA 01703 - Attn: R. Greenberg (1 copy)
Science Applications, Inc., P.O. Box 2351, La Jolla, CA 92037 - Attn: Dr. John Asmus (1 copy)
Systems Science and Software, P.O. Box 1620, La Jolla, CA 92037 - Attn: Alan F. Klein (1 copy)
Systems Consultants, Inc., 1050 31st Street, NW, Washington, D.C. 20007 - Attn: Dr. R. B. Keller (1 copy)
Thiokol Chemical Corp., Wasatch Division, P.O. Box 524, Brigham City, UT 84302 - Attn: Mr. J. E. Hansen (1 copy)
TRW Systems Group, One Space Park, Bldg. R-1, Rm. 1050, Redondo Beach, CA 90278 - Attn: Mr. Norman Campbell (1 copy)
United Technologies Research Center, 400 Main Street, East Hartford, Ct. 06108 - Attn: Mr. G. H. McLafferty (1 copy)
United Technologies Research Center, Pratt and Whitney Aircraft Div., Florida R&D Center, West Palm Beach, FL 33402 - Attn: Dr. R. A. Schmidke (1 copy)
Mr. Ed Pinsley (1 copy)
Varian Associates, EIMAC Division, 301 Industrial Way, San Carlos, CA 94070 - Attn: Mr. Jack Quinn (1 copy)
Vought Systems Division, LTV Aerospace Corp., P. O. Box 5907, Dallas, TX 75222 - Attn: Mr. F. G. Simpson, MS254142 (1 copy)

DISTRIBUTION LIST (Continued)

Westinghouse Electric Corp., Defense and Space Center, Balt-Wash. International Airport, Box 746, Baltimore, MD 21203 - Attn: Mr. W. F. List (1 copy)
Westinghouse Research Labs, Beulah Road, Churchill Boro, Pittsburgh, PA 15235 - Attn: Dr. E. P. Riedel (1 copy)
United Technologies Research Center, East Hartford, CT 06108 - Attn: A. J. De Maria (1 copy)
Aireborne Instruments Laboratory, Walt Whitorian Road, Melville, NY 11746 - Attn: F. Pace (1 copy)
General Electric R&D Center, Schenectady, NY 12305 - Attn: Dr. Donald White (1 copy)
Cleveland State University, Cleveland, OH 44115 - Attn: Dean Jack Soules (1 copy)
Exxon Research and Engineering Co., P. O. Box 8, Linden, NJ 07036 - Attn: D. Grafstein (1 copy)
University of Maryland, Department of Physics and Astronomy, College Park, MD 20742 - Attn: D. Currie (1 copy)
Sylvania Electric Products Inc., 100 Fergeson Drive, Mountain View, CA 94040 - Attn: L. M. Osterink (1 copy)
North American Rockwell Corp., Autonetics Division, 3370 Miraloma Avenue, Anaheim, CA 92803 - Attn: R. Gudmundsen (1 copy)
Massachusetts Institute of Technology, 77 Massachusetts Avenue, Cambridge, MA 02138 - Attn: Prof. A. Javan (1 copy)
Lockheed Missile & Space Co., Palo Alto Research Laboratories, Palo Alto, CA 94304 - Attn: Dr. R. C. Ohlman (1 copy)
Polytechnic Institute of New York, Rt. 110, Farmingtondale, NY 11735 - Attn: Dr. William T. Walter (1 copy)